

Abstract

Organic aerosol concentrations are simulated using the WRF-CHEM model in Mexico City during the period from 24 to 29 March in association with the MILAGRO-2006 campaign. Two approaches are employed to predict the variation and spatial distribution of the organic aerosol concentrations: (1) a traditional 2-product secondary organic aerosol (SOA) model with non-volatile primary organic aerosols (POA); (2) a non-traditional SOA model including the volatility basis-set modeling method in which primary organic components are assumed to be semi-volatile and photochemically reactive and are distributed in logarithmically spaced volatility bins. The MCMA 2006 official emission inventory is used in simulations and the POA emissions are modified and distributed by volatility based on dilution experiments for the non-traditional SOA model. The model results are compared to the Aerosol Mass Spectrometry (AMS) observations analyzed using the Positive Matrix Factorization (PMF) technique at an urban background site (T0) and a suburban background site (T1) in Mexico City. The traditional SOA model frequently underestimates the observed POA concentrations during rush hours and overestimates the observations in the rest of the time in the city. The model also substantially underestimates the observed SOA concentrations, particularly during daytime, and only produces 21% and 25% of the observed SOA mass in the suburban and urban area, respectively. The non-traditional SOA model performs well in simulating the POA variation, but still overestimates during daytime in the urban area. The SOA simulations are significantly improved in the non-traditional SOA model compared to the traditional SOA model and the SOA production is increased by more than 100% in the city. However, the underestimation during daytime is still salient in the urban area and the non-traditional model also fails to reproduce the high level of SOA concentrations in the suburban area. In the non-traditional SOA model, the aging process of primary organic components considerably decreases the OH levels in simulations and further impacts the SOA formation. If the aging process in the non-traditional model does not have feedback on the OH in the gas-phase chemistry,

Simulations of organic aerosol concentrations in Mexico City

G. Li et al.

Title Page

Abstract

Introduction

Conclusions

References

Tables

Figures

⏪

⏩

◀

▶

Back

Close

Full Screen / Esc

Printer-friendly Version

Interactive Discussion



**Simulations of
organic aerosol
concentrations in
Mexico City**

G. Li et al.

Title Page

Abstract

Introduction

Conclusions

References

Tables

Figures

⏪

⏩

◀

▶

Back

Close

Full Screen / Esc

Printer-friendly Version

Interactive Discussion



the SOA production is enhanced by more than 10% compared to the simulations with the OH feedback during daytime, and the gap between the simulations and observations in the urban area is around $3 \mu\text{g m}^{-3}$ or 20% on average during late morning and early afternoon, within the uncertainty from the AMS measurements and PMF analysis. In addition, glyoxal and methylglyoxal can contribute up to approximately 10% of the observed SOA mass in the urban area and 4% in the suburban area. Including the non-OH feedback and the contribution of glyoxal and methylglyoxal, the non-traditional SOA model can explain up to 83% of the observed SOA in the urban area, and the underestimation during late morning and early afternoon is reduced to $0.9 \mu\text{g m}^{-3}$ or 6% on average. Considering the uncertainties from measurements, emissions, meteorological conditions, aging of SOA from anthropogenic VOCs, and contributions from background transport, the non-traditional SOA model is capable of closing the gap in SOA mass between measurements and models.

1 Introduction

Atmospheric aerosols influence the radiative balance in Earth's atmosphere and play a central role in climate, directly by scattering or absorbing a fraction of the incoming solar radiation to cool or warm the atmosphere, and indirectly via their roles as cloud condensation nuclei (CCN) and ice nuclei (IN), by modifying optical properties and lifetime of clouds (e.g., Penner et al., 2001; Zhang et al., 2007a). Additionally, high levels of particulate matter are associated with adverse human effects, including increased morbidity and mortality arising from altered respiratory and cardiovascular function (e.g., Pope and Dockery, 2006; Harrison and Yin, 2000; Davidson et al., 2005).

Organic aerosols (OA) account for 20–90% of the total fine particulate mass in the atmosphere (Zhang et al., 2007b) and potentially play an important role in climate and human health (Pope and Dockery, 2006). Generally, OA is categorized into two types: primary OA (POA) that is directly emitted into the atmosphere in particulate form, and secondary OA (SOA) which is formed from chemically processed gaseous organic

on the measurements taken during MCMA-2006. The WRF-CHEM model and the model configuration are described in Sect. 2. Results of the modeling experiments and comparisons are presented in Sect. 3, and the Conclusions are given in Sect. 4.

2 Model description

2.1 WRF-CHEM model

The version of the WRF-CHEM model used in the present study was developed by Li et al. (2010) at the Molina Center for Energy and the Environment, with a new flexible gas phase chemical module that can be utilized in different chemical mechanisms, including CB-IV, RADM2, and SAPRC. The gas-phase chemistry differential equations are solved by an Euler backward Gauss-Seidel iterative technique. The short-lived species, such as OH and O(¹D), are assumed to be in steady state. The solution is iterated until all species are within 0.1% of their previous iterative values. For the aerosol simulations, the CMAQ (version 4.6) aerosol module developed by EPA, which is designed to be an efficient and economical depiction of aerosol dynamics in the atmosphere (Binkowski and Roselle, 2003), is implemented in the WRF-CHEM model. In this aerosol module, the particle size distribution is represented as the superposition of three lognormal sub-distributions called modes. The processes of coagulation, particle growth by the addition of mass, and new particle formation are included. In addition, the wet deposition also follows the method used in CMAQ. Surface deposition of chemical species is parameterized following Wesely (1989). The photolysis rates are calculated using the Fast Tropospheric Ultraviolet and Visible (FTUV) Radiation Model (Tie et al., 2003; Li et al., 2005).

Li et al. (2010) have found that HONO sources play an important role in early morning photochemistry and the formation of secondary aerosols via photolysis to form OH. The HONO sources suggested by Li et al. (2010) have been considered in this study to enhance the OH concentration. In addition, two additional OH sources are also

Simulations of organic aerosol concentrations in Mexico City

G. Li et al.

Title Page

Abstract

Introduction

Conclusions

References

Tables

Figures

⏪

⏩

◀

▶

Back

Close

Full Screen / Esc

Printer-friendly Version

Interactive Discussion



incorporated in the WRF-CHEM model. The first one is the reaction of excited NO₂ with H₂O (Li et al., 2008):



10 The rate constants used are $k_2 = 3.3 \times 10^{-11}$, $k_3 = 2.7 \times 10^{-11}$, $k_{4a} = 1.7 \times 10^{-10}$, and $k_{4b} = 1.7 \times 10^{-13} \text{ cm}^3 \text{ molec}^{-1} \text{ s}^{-1}$. Time-resolved photolysis frequencies for Reaction (R1) are calculated using NO₂ absorption cross sections, quantum yields for the production of excited molecules of NO₂ and values of the actinic flux (320–645 nm). Absorption cross sections and quantum yields are taken from the FTUV model (Tie et al., 2003). The second OH source is peroxy radical reactions such as:



where α is assumed to be 0.5 (Lelieveld et al., 2008).

2.2 Secondary organic aerosol models

20 Two types of SOA models are considered in the WRF-CHEM model: a traditional two-product SOA model (T2-SOA model) adopted from CMAQ (Binkowski and Roselle, 2003), and a non-traditional SOA model (NT-SOA model) developed by Tsimpidi et al. (2010).

Simulations of organic aerosol concentrations in Mexico City

G. Li et al.

Title Page

Abstract

Introduction

Conclusions

References

Tables

Figures

⏪

⏩

◀

▶

Back

Close

Full Screen / Esc

Printer-friendly Version

Interactive Discussion



2.2.1 T2-SOA model

In the T2-SOA model, the SOA concentrations are simulated from the oxidation of six primary organic gases (POG): alkanes, alkenes, cresol, high-yield aromatics, low-yield aromatics, and monoterpenes. Ten semi-volatile organic compounds (SVOC) are produced via these reactions – two each for olefins, monoterpenes, and aromatics, and one each for alkanes and cresol.



The oxidants mainly include the OH radical, the nitrate radical NO_3 , and O_3 . The saturation vapor pressures and mass-based stoichiometric yield coefficients (α_i) of SVOCs are obtained from either smog chamber experiments or from published estimates in cases where smog chamber data are unavailable. The SOA is calculated using the method developed by Schell et al. (2001), which was based on the absorptive partitioning model of Pankow (1994) that was extended by Odum et al. (1996). When the organic gas/aerosol equilibrium has been established, gas and aerosol-phase concentrations of each SVOC are calculated iteratively using a globally convergent variation of Newton's method.

2.2.2 NT-SOA model

In the NT-SOA model, the volatility basis-set approach (Lane et al., 2008a) is used to consider the SOA formation, assuming that primary organic components are semi-volatile and photochemically reactive and are distributed in logarithmically spaced volatility bins. The partitioning of semi-volatile organic species is calculated using the algorithm suggested by Koo et al. (2003), in which the bulk gas and particle phases are in equilibrium and all condensable organics form a pseudo-ideal solution (Odum et al., 1996). Nine surrogate species with saturation concentrations from 10^{-2} to $10^6 \mu\text{g m}^{-3}$ at room temperature are used for the POA components following the approach of Shrivastava et al. (2008).

29356

ACPD

10, 29349–29404, 2010

Simulations of organic aerosol concentrations in Mexico City

G. Li et al.

Title Page

Abstract

Introduction

Conclusions

References

Tables

Figures

⏪

⏩

◀

▶

Back

Close

Full Screen / Esc

Printer-friendly Version

Interactive Discussion



Simulations of organic aerosol concentrations in Mexico City

G. Li et al.

Title Page

Abstract

Introduction

Conclusions

References

Tables

Figures

⏪

⏩

◀

▶

Back

Close

Full Screen / Esc

Printer-friendly Version

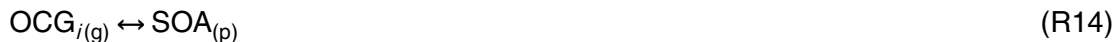
Interactive Discussion



Based on the volatility basis-set approach, the SOA formation from each anthropogenic or biogenic precursor is predicted using four SOA species whose effective saturation concentrations at 298 K are 1, 10, 100, and 1000 $\mu\text{g m}^{-3}$, respectively, instead of the traditional 2-product parameterization. The anthropogenic aerosol yields have been updated based on laboratory results from recent smog-chamber experiments (Ng et al., 2006; Hildebrandt et al., 2009) and are NO_x -dependent (Lane et al., 2008b). Under low- NO_x conditions, RO_2 radicals react with other peroxy radicals to form a distribution of products with lower volatilities, resulting in higher SOA yields. However, when the NO_x concentrations are high, the SOA yields are lower because RO_2 predominantly reacts with NO and the products distribution is dominated by aldehydes, ketones, and nitrates.

In this new approach, all primary species are treated as chemically reactive. Primary organic gases (POG), emitted or formed due to evaporation of POA in the atmosphere (Robison et al., 2007), are assumed to react with OH radicals to reduce their volatility and hence to partition between gas and particle phase forming SOA. Intermediate volatility species (IVOC), which are co-emitted with the POA but are never in the particle phase during the emission process, are also oxidized by OH to form SOA. The POA and IVOC aging process is modeled using a gas-phase OH reaction with a rate constant of $4 \times 10^{-11} \text{ cm}^3 \text{ molec}^{-1} \text{ s}^{-1}$ (Atkinson and Arey, 2003). Each reaction is assumed to reduce the volatility of the vapor material by an order of magnitude (e.g., shifting material from a C^* of 100 to 10 $\mu\text{g m}^{-3}$), with a small net increase in mass (7.5%) to account for added oxygen. In the base case, we assume that the organic condensable gases (OCG) produced from the oxidation of anthropogenic and biogenic VOCs do not react further with OH radicals to reduce the volatility. Tsimpidi et al. (2010) and Murphy and Pandis (2009) have assumed that these first generation products continue to react and age. The importance of this anthropogenic SOA aging process will be explored in a sensitivity test in a subsequent section. The base case reaction scheme is represented by the reactions below:





where i is the corresponding volatility bin. Detailed description about the volatility basis-set approach can be found in Tsimpidi et al. (2010). Furthermore, when the volatility basis-set approach is used in simulations, the POA emissions are redistributed following the base case suggested by Tsimpidi et al. (2010). The total amount of material (POA + SVOC + IVOC) introduced in the NT-SOA model is 7.5 times of the particle-phase POA emissions.

2.3 Model configuration

A six-day episode from 24 to 29 March 2006 is selected in the present study, including a typical “O₃-Convection South” condition (24–26 March) and “O₃-Convection North” condition (27–29 March) in Mexico City (de Foy et al., 2008). The WRF-CHEM model is configured with grid spacing of 3 km (99 × 99 grid points) centered at 19.538° N and 99° E (Fig. 1). Thirty-five vertical levels are used in a stretched vertical grid with spacing ranging from 50 m near the surface, to 500 m at 2.5 km a.g.l. and 1 km above 14 km. The modeling system employs the Lin microphysics scheme (Lin et al., 1983), the Yonsei University (YSU) PBL scheme (Noh et al., 2001), the Noah land-surface model (Chen and Dudhia, 2001), a longwave radiation parameterization (Mlawer et al., 1997),

Simulations of organic aerosol concentrations in Mexico City

G. Li et al.

Title Page

Abstract

Introduction

Conclusions

References

Tables

Figures

◀

▶

◀

▶

Back

Close

Full Screen / Esc

Printer-friendly Version

Interactive Discussion



Simulations of organic aerosol concentrations in Mexico City

G. Li et al.

Title Page

Abstract

Introduction

Conclusions

References

Tables

Figures

⏪

⏩

◀

▶

Back

Close

Full Screen / Esc

Printer-friendly Version

Interactive Discussion



and a shortwave radiation parameterization (Dudhia, 1989). Meteorological initial and boundary conditions are obtained from NCEP $1^\circ \times 1^\circ$ reanalysis data. Chemical initial and boundary conditions are interpolated from MOZART 3-hour output (Horowitz et al., 2003). The SOA initial conditions are set to be $0.5 \mu\text{g m}^{-3}$ according to the measurements on 24 March 2006 at T0 and T1 sites, and the boundary conditions in the boundary layer are set to be $1.4 \mu\text{g m}^{-3}$ according to the previous studies in Mexico City (Hodzic et al., 2009; Dzepina et al., 2009).

The emission inventory (EI) used in the present study is based on the 2006 official EI for the MCMA and adjusted according to observations, as described in Song et al. (2010). The emissions of the lumped species ARO2 are not adjusted, as Song et al. (2010) have found that the adjusted ARO2 emissions are still probably underestimated. An anthropogenic emission source is added to isoprene equal to 0.014 time of the ethylene emissions (Borbon et al., 2001; Hodzic et al., 2009) to improve the isoprene simulation during rush hours. The OA emissions in the present EI do not include the contributions from biomass burning in the modeling domain. Therefore, for the evaluation of OA simulations, we have chosen the above-described six-day episode that has been reported to have less impacts from biomass burning during the MILAGRO campaign (Aiken et al., 2009).

2.4 Measurements and statistical methods for comparisons

During the MCMA-2006/MILAGRO Campaign, an extensive set of measurements of gas and aerosol pollutant concentrations was obtained from ground-based platforms, aircraft and satellites (Molina et al., 2010). Comparisons of surface O_3 and CO are made using the measurements collected by the Mexico City Ambient Air Monitoring Network (RAMA). VOCs measurements at T0 from LP-DOAS and PTR-MS are used to verify the EI in Mexico City (Zheng et al., 2008; Song et al., 2010). The simulated organic aerosols in the WRF-CHEM model are compared with the AMS data analyzed using PMF at T0 and T1 (Aiken et al., 2009). The AMS OA is separated into three components: the hydrocarbon-like organic aerosol (HOA), which is a surrogate

of fresh POA; the oxidized organic aerosol (OOA), which is interpreted as a surrogate of SOA and reacted POA; and the biomass burning organic aerosol (BBOA). The absolute uncertainty of the AMS concentrations is $\pm 25\%$ and is dominated by the uncertainty in particle collection efficiency according to Jimenez et al. (2003) and DeCarlo et al. (2008), while the relative uncertainty in the separation of PMF components is of the order of 10%.

In order to evaluate the overall performance of the WRF-CHEM model in simulating gas-phase species and aerosols against measurements, the normalized mean bias (NMB), the root mean square error (RMSE), and the index of agreement (IOA) are used in the present study.

$$\text{NMB} = \frac{\sum_{i=1}^N (P_i - O_i)}{\sum_{i=1}^N O_i} \quad (\text{R15})$$

$$\text{RMSE} = \left[\frac{1}{N} \sum_{i=1}^N (P_i - O_i)^2 \right]^{\frac{1}{2}} \quad (\text{R16})$$

$$\text{IOA} = 1 - \frac{\sum_{i=1}^N (P_i - O_i)^2}{\sum_{i=1}^N (|P_i - \bar{O}| + |O_i - \bar{O}|)^2} \quad (\text{R17})$$

where P_i and O_i are the predicted and observed pollutant concentration, respectively. N is the total number of the predictions used for comparisons, and \bar{O} denotes the average of the observation. The IOA ranges from 0 to 1, with 1 indicating perfect agreement between model and observation.

Simulations of organic aerosol concentrations in Mexico City

G. Li et al.

Title Page

Abstract

Introduction

Conclusions

References

Tables

Figures

◀

▶

◀

▶

Back

Close

Full Screen / Esc

Printer-friendly Version

Interactive Discussion



3 Results and discussions

3.1 Model performance

3.1.1 O₃ and CO comparisons with ambient measurements

5 Simulated O₃ and CO concentrations from the NT-SOA model are compared with the RAMA observations. Since meteorological conditions play a key role in air pollution simulations principally through determining the dispersion or accumulation of pollutant emissions (Bei et al., 2008, 2010), in Fig. 2, we present the spatial distributions of calculated and observed near-surface concentrations of O₃ at 14:00 and 17:00 Local Time (LT) from 24 to 29 March 2006, along with the simulated wind fields. Generally, at 14:00 LT, the predicted O₃ spatial patterns agree well with the observations at the ambient monitoring sites. On 24 March, the stagnant conditions in the basin are favorable for the buildup of high O₃ concentrations. The predicted O₃ concentrations exceed 80 ppb within almost the entire basin and are in good agreement with RAMA measurements. On 25 March, the noontime winds from the northwest of the basin are well organized and commence to evacuate the pollutants in the basin. The divergence of the pollutants in the basin causes the low O₃ concentrations in the central part of the basin, reasonably consistent with the measurements. On 26 March, the light and disordered winds in the basin are contributed to the development of high O₃. The well organized northwest winds have impacted the plumes formed in the basin during noontime. During 27 to 29 March, the WRF-CHEM model successfully reproduces the movement of O₃ plumes to the northwest, which are forced by the well organized south and northeast winds from outside of the basin. At 17:00 LT (Fig. 2b), on 24 and 25 March, the clean air from the northwest of the basin has been transported into the basin and the simulated O₃ concentrations decrease to 40–60 ppb, comparable with the observations. However, on 26 March, the convergence in the basin keeps the O₃ plume stagnant in the basin, leading to the overestimation of the observed O₃ concentrations. On 27 March, the strong southern winds push the plume to the north of the

Simulations of organic aerosol concentrations in Mexico City

G. Li et al.

Title Page

Abstract

Introduction

Conclusions

References

Tables

Figures

⏪

⏩

◀

▶

Back

Close

Full Screen / Esc

Printer-friendly Version

Interactive Discussion



basin and the model reasonably well reproduces the observed O₃ distribution. On 28 and 29 March, the simulated plumes move slowly compared with the observations. For example, on 29 March, the observed plume had moved to the north of the basin, but part of the modeled plume remains stagnant in the center of the city.

5 Figure 3 shows the diurnal variations of simulated and observed near-surface O₃ and CO concentrations averaged over the RAMA monitoring sites. The WRF-CHEM model generally tracks the temporal variations of O₃ concentrations reasonably well during daytime (Fig. 3a). The NMB and RMSE are 20% and 11 ppb, respectively, and the IOA reaches 95%, indicating good agreement of O₃ simulations with measurements. On 24 and 27 March, the model reproduces successfully the daytime variations of O₃ concentrations. In the remaining four days, the model is capable of replicating the rapid increase of morning O₃ concentrations and the falloff of afternoon O₃ levels, but the overestimation of O₃ concentrations still exists in the afternoon, which is attributed principally to the slow movement of the plumes. Although the low nighttime O₃ concentrations due to the titration of emitted NO are reproduced, the nighttime simulated O₃ deviates considerably from the observations, except on 26 March, because of difficulties in modeling the meteorological fields during the night and the complexity of the nighttime chemistry (Li et al., 2007; Zhang et al., 2009). In Fig. 3b, the model follows well the variation of CO concentrations during daytime in general, but it frequently overestimates CO concentrations during nighttime, indicating either the failure of PBL simulations or inefficiency of the pollutant dispersion process or problems with the emissions during nighttime (Zhang et al., 2009). The NMB and RMSE are 10% and 0.5 ppm, respectively, and the IOA reduces to 84% compared to the O₃ simulations. The good agreement between the long-lived predicted CO and the corresponding measurements suggests that the model simulates reasonably well the meteorological fields and the corresponding emissions during daytime.

Simulations of organic aerosol concentrations in Mexico City

G. Li et al.

[Title Page](#)[Abstract](#)[Introduction](#)[Conclusions](#)[References](#)[Tables](#)[Figures](#)[⏪](#)[⏩](#)[◀](#)[▶](#)[Back](#)[Close](#)[Full Screen / Esc](#)[Printer-friendly Version](#)[Interactive Discussion](#)

3.1.2 Organic aerosol simulations at T0 and T1

Figure 4 presents the comparison of modeled and PMF results (called “observed” from now on even if they are really the results of an observation-based model) diurnal variations of POA and SOA concentrations at T0 and T1. The T2-SOA model simulates the POA diurnal variations reasonably well at T0 and T1 when the POA is non-volatile (Fig. 4a and c). However, the T2-SOA model significantly underestimates the observed POA during rush hours throughout the entire episode at T1 and on 28th and 29th at T0, suggesting that the EI misses local sources near T1. In addition, the T2-SOA model frequently overestimates the measured daytime POA at T0 and T1. The IOA of POA is 0.81 and 0.59 at T0 and T1 (Table 1), respectively, reasonably reflecting the performance of the T2-SOA model in simulating the POA variations at the two sites.

Hodzic et al. (2009) have used an air quality model to explore the processes controlling organic aerosols in the vicinity of Mexico City. Their model has reasonably reproduced the observed concentrations of POA at T0 and T1 with the non-volatile POA assumption. Their model results on POA are also in a good agreement with the study by Fast et al. (2009), who have also modeled during MILAGO and considered POA as non-volatile. It is worthy to note that Hodzic et al. (2009) and Fast et al. (2009) have used the same 2002 MCMA emissions inventory as adjusted by Lei et al. (2007). Although an updated 2006 MCMA inventory has been utilized in this study, our POA simulations are comparable to those reported by Hodzic et al. (2009) and Fast et al. (2009) when the POA is considered as non-volatile.

When POA is assumed to be semi-volatile (Robinson et al., 2007) and adjusted and redistributed as Tsimpidi et al. (2010) in the NT-SOA model, the simulation of POA is improved compared with the results from the T2-SOA model during almost the entire period against the measurement at T0, with the IOA increasing from 0.81 to 0.85. The POA level in the NT-SOA model is higher during rush hours and slightly lower in the noontime and afternoon compared to the results from the T2-SOA model, and are more consistent with the observations. As T0 is located near the urban center of Mexico City,

Simulations of organic aerosol concentrations in Mexico City

G. Li et al.

Title Page

Abstract

Introduction

Conclusions

References

Tables

Figures



Back

Close

Full Screen / Esc

Printer-friendly Version

Interactive Discussion



the traditional SOA model still fails to yield sufficient SOA concentrations to match the observations by a factor of 7. Hodzic et al. (2009) also reported that less than 15% of the observed SOA within Mexico City can be explained by the traditional mechanism based on oxidation of anthropogenic precursors.

On the other hand, the NT-SOA model significantly improves the SOA simulations at T0 compared to those from the T2-SOA model with about 100% enhancement of the SOA production, but the predicted SOA is still lower during daytime by a factor of about 2 compared to the PMF results. The SOA production from anthropogenic precursors is increased by 33% in the NT-SOA model compared to the T2-SOA model, indicating the high formation of SOA from anthropogenic aromatics in the NT-SOA model (Hildebrandt et al., 2009), and contributes 36% of the predicted SOA concentrations during the six-day simulation period. The most important source of the predicted SOA concentrations is the aging of the semi-volatile POA, with about 45% contribution. The biogenic precursors also provide 19% of the predicted SOA concentrations. On average, the NT-SOA model produces about 50% of the observed SOA at T0 during the simulation period. In the case study of Dzepina et al. (2009) in Mexico City, if the mechanism in Robinson et al. (2007) is included, they can close the gap in SOA mass between measurements and models with large contribution of SOA from glyoxal. However, in the present study, although the NT-SOA model has included the SOA contributions from semi-volatile POA and high yield of SOA formation from anthropogenic aromatics, there still exist considerably large discrepancies between measurements and models during daytime, particularly in the morning. On average, the T2-SOA and NT-SOA model both underestimate the observed SOA at T0, with the NMB of -57% and -33%, respectively, although the NT-SOA model performs much better than the T2-SOA model, with the IOA increased from 0.49 to 0.70 and the RMSE decreased from 7.0 to 5.0 $\mu\text{g m}^{-3}$.

At T1, the observed SOA exhibits distinctly two peaks in the morning and afternoon. The T2-SOA model severely underestimates the observed SOA concentrations during daytime and can only explain 21% of the observation. The NT-SOA model fails to

Simulations of organic aerosol concentrations in Mexico City

G. Li et al.

Title Page

Abstract

Introduction

Conclusions

References

Tables

Figures



Back

Close

Full Screen / Esc

Printer-friendly Version

Interactive Discussion



produce the first peak in the morning and also underestimates the second peak in the afternoon, which is due to the outflow from the polluted urban area that the model fails to predict accurately. The NT-SOA model predicts 32% of the observed SOA mass at T1, about 50% more than that from the T2-SOA model. About 15% of the predicted SOA concentrations are contributed by the anthropogenic precursors during the six-day period. The biogenic precursors provide 30% of the predicted SOA concentrations, more than that from the anthropogenic precursors, demonstrating the significant contribution of SOA from biogenic sources at the suburban background site T1. The aging of the semi-volatile POA contributes about 55% of the predicted SOA concentrations.

Based on the above comparison, the NT-SOA model simulates well the POA concentrations at T0, but underestimates during rush hours at T1, which might be caused by the uncertainties of local POA emissions or meteorological conditions. Although the NT-SOA model incorporates the recently suggested SOA mechanisms, it still underestimates the SOA concentrations at T0 and T1 during daytime, which is plausibly attributed to the conditions used in simulations, such as meteorological fields, boundary conditions, emissions, OH treatment, aging of SOA from anthropogenic precursors, etc. One of the most important factors dominating the performance of air quality models is the simulation of meteorological fields. However, according to the O₃ and CO simulations, the WRF-CHEM model generally exhibits a good performance in simulating the plume formation and movement during daytime, indicating the reasonable simulations of meteorological fields. In the following sections, we will discuss the uncertainties except from meteorological fields in the SOA simulations.

3.2 Uncertainties in SOA simulations

3.2.1 Emissions inventory

The uncertainties in emissions inventory directly influence the simulation of the SOA precursors and the formation of SOA in air quality models. In the SAPRC99 chemical mechanism used in the study, the major anthropogenic SOA precursors are

Simulations of organic aerosol concentrations in Mexico City

G. Li et al.

Title Page

Abstract

Introduction

Conclusions

References

Tables

Figures



Back

Close

Full Screen / Esc

Printer-friendly Version

Interactive Discussion



aromatics, lumped into ARO1 and ARO2. ARO1 mainly includes toluene, benzene, ethylbenzene, and other aromatics with the reaction rate with OH (k_{OH}) less than $2 \times 10^4 \text{ ppm}^{-1} \text{ min}^{-1}$. ARO2 includes xylene, trimethylbenzene, and other aromatics with k_{OH} greater than $2 \times 10^4 \text{ ppm}^{-1} \text{ min}^{-1}$. Figure 5a shows the comparison of simulated ARO1 with the total of observed toluene, benzene, and ethylbenzene at T0. The WRF-CHEM model generally follows the variation of the total of observed toluene, benzene, and ethylbenzene from 24 to 26 March, but overestimates during daytime. During the period from 27 to 29 March, the model performs reasonably well in simulating the observations but underestimates during rush hours on 28th and 29th. The averaged simulated ARO1 at T0 during the six-day episode is 12.6 ppb, close to the observed 12.2 ppb. In Fig. 5b, the simulated ARO2 is compared with the total of observed m-xylene, o-xylene, p-xylene, naphthalene, and 135-trimethylbenzene. In general, the WRF-CHEM model successfully reproduces the variability of the observation during daytime but often underestimates. The averaged simulated ARO2 is about 10.4 ppb, less than the observed 14.5 ppb, which is consistent with the results in Song et al. (2010).

Monoterpene and isoprene are the main biogenic precursors considered in the SAPRC99 chemical mechanism. Figure 6 presents the comparison of modeled and PTR-MS observed monoterpene and isoprene at T0 during the period of 24–29 March. The observed peak isoprene concentrations occur during traffic rush hours, showing a strong anthropogenic signature (Hodzic et al., 2009). Therefore, when an anthropogenic source of isoprene as suggested by Borbon et al. (2001) is included, the model successfully reproduces the isoprene peak in the morning (Fig. 6a). However, the model frequently overestimates the observation in the evening, which is attributed to the transport of isoprene from the mountains surrounding Mexico City. The model substantially underestimates monoterpene concentrations during daytime and also fails to simulate the observed peak time in the early morning (Fig. 6b). However, considering the observed low level of monoterpene during daytime, the underestimation of monoterpene might not contribute significantly to the SOA evaluation.

Simulations of organic aerosol concentrations in Mexico City

G. Li et al.

[Title Page](#)[Abstract](#)[Introduction](#)[Conclusions](#)[References](#)[Tables](#)[Figures](#)[⏪](#)[⏩](#)[◀](#)[▶](#)[Back](#)[Close](#)[Full Screen / Esc](#)[Printer-friendly Version](#)[Interactive Discussion](#)

The simulated POA concentrations in the T2-SOA and NT-SOA models are comparable to the measurement at T0, indicating that the POA emissions used in this study are generally reasonable in the urban area. Hence, from the point of view of the EI, the underestimation of ARO2 contributes to one of the important uncertainties in the evaluation of SOA formation.

3.2.2 SOA contributions from dicarbonyl compounds

Recent chamber experiments have indicated that dicarbonyl compounds, such as glyoxal and methylglyoxal, may play a role in the SOA formation via aerosol uptake and cloud processing (e.g., Carlton et al., 2006, 2007; Zhao et al., 2006). Volkamer et al. (2007) and Dzepina et al. (2009) have suggested that the contribution of glyoxal can explain at least 15% of the SOA formation in Mexico City. Fu et al. (2009) have found that inclusion of dicarbonyl SOA doubles the SOA contribution to water soluble organic carbon aerosol at all altitudes over eastern North America. Considerable uncertainty remains regarding the irreversible uptake coefficient of glyoxal on aerosol surfaces, varying from 4×10^{-4} to 7.3×10^{-3} (Liggio et al., 2005; Volkamer et al., 2007; De Hann et al., 2009). Although the irreversible uptake for methylglyoxal is still controversial, recent studies have supported its potential role in SOA formation (Zhao et al., 2006; Sareen et al., 2010). In this study, the SOA formation from glyoxal and methylglyoxal is parameterized as a first-order irreversible uptake by aerosol particles, with a reactive uptake coefficient of 3.7×10^{-3} for glyoxal and methylglyoxal (Liggio et al., 2005; Zhao et al., 2006; Volkamer et al., 2007).

Figure 7a and b show the temporal variation of SOA concentrations from glyoxal and methylglyoxal at T0 and T1. At T0, glyoxal has its largest contribution to the SOA formation on 24 March, about $1.2 \mu\text{g m}^{-3}$. The contribution from methylglyoxal is more than that from glyoxal. On average, the irreversible uptake of glyoxal can explain about 2.7% of the observed SOA mass at T0 and the contribution from methylglyoxal can be up to 3.3%. Dzepina et al. (2009) have used a photochemical box model to evaluate the contribution of several recently proposed SOA mechanisms to the SOA formation

Simulations of organic aerosol concentrations in Mexico City

G. Li et al.

Title Page

Abstract

Introduction

Conclusions

References

Tables

Figures

⏪

⏩

◀

▶

Back

Close

Full Screen / Esc

Printer-friendly Version

Interactive Discussion



in a case study during MCMA-2003. They have found that the amount of SOA from glyoxal explains about 17% of observed SOA mass. The case investigated by Dzepina et al. (2009) is similar to that occurring on 24 March in this study in terms of meteorology and the SOA development. However, in the simulation with the NT-SOA model, glyoxal only contributes 3.5% to the observed SOA during the time period from 00:00 to 14:00 LT, only about 20% of the estimation by Dzepina et al. (2009). It is worthy to note that the WRF-CHEM model underestimates the glyoxal concentrations compared to the measurement at T0 (Fig. 7c), which can partially explain the lower SOA production. Additionally, in the study of Dzepina et al. (2009), the modeled gas-phase glyoxal was 2–6 times higher than the direct DOAS measurements, which caused much more SOA formation from glyoxal when Henry's law is used to partition gas-phase glyoxal into aerosol liquid water with an effective constant $H_{\text{eff}} = 4 \times 10^9 \text{ M atm}^{-1}$, constrained by the observed glyoxal. At T1, the contribution of glyoxal and methylglyoxal to the SOA formation is small, less than 2% of the observation (Fig. 7b).

3.2.3 Uncertainties from SOA formation mechanisms

The mechanism of Robinson et al. (2007) is used in the NT-SOA model to account for the SOA production from the aging of semi-volatile POA. Grieshop et al. (2009) has proposed a variation of the mechanism based on the evolution of chamber SOA from wood smoke that has a similar distribution of semi-volatile species as diesel emissions. In the new mechanism, every generation of oxidation decreases the saturation concentration (C^*) of the products by two orders of magnitude per oxidation step and the mass increase per oxidation step is 40% but the oxidation rates with OH is decreased to $2 \times 10^{-11} \text{ cm}^3 \text{ molec}^{-1} \text{ s}^{-1}$. In addition, in the mechanism of Robinson et al. (2007), the enthalpy of vaporization for calculation of C^* ranges from 112 to 64 kJ mol^{-1} , but it is decreased to 77–46 kJ mol^{-1} in the mechanism of Grieshop et al. (2009).

The new mechanism is also incorporated into the NT-SOA model, which is referred to as the NT2-SOA model. A sensitivity study is conducted using the NT2-SOA model with the same initial and boundary conditions as the NT-SOA model. As shown in

Simulations of organic aerosol concentrations in Mexico City

G. Li et al.

Title Page

Abstract

Introduction

Conclusions

References

Tables

Figures

⏪

⏩

◀

▶

Back

Close

Full Screen / Esc

Printer-friendly Version

Interactive Discussion



**Simulations of
organic aerosol
concentrations in
Mexico City**

G. Li et al.

Title Page

Abstract

Introduction

Conclusions

References

Tables

Figures

⏪

⏩

◀

▶

Back

Close

Full Screen / Esc

Printer-friendly Version

Interactive Discussion



Fig. 8a and c, the NT2-SOA model generally produces less POA mass than the NT-SOA model at T0 and T1, especially during nighttime and rush hours, which is caused by the decrease of the enthalpy of vaporization of POG in the NT2-SOA model. The decrease of the enthalpy increases C^* of POG, leading to less POG in the particle phase.

Compared to the NT-SOA model, the NT2-SOA model slightly improves the POA simulation at T0, with the RMSE decreased from 3.8 to 3.5 $\mu\text{g m}^{-3}$ and IOA increased from 0.85 to 0.86. The NT2-SOA model considerably improves the SOA production compared to the NT-SOA model at T0, with the IOA increased from 0.70 to 0.83 and the RMSE decreased from 5.0 to 4.0 $\mu\text{g m}^{-3}$ (Fig. 8b). On average, the SOA mass in the NT2-SOA model is increased by 1.2 $\mu\text{g m}^{-3}$ compared to the NT-SOA model, which is principally attributed to the aging of the semi-volatile POA (about 1.1 $\mu\text{g m}^{-3}$). Although the oxidation rates of semi-volatile species with OH are decreased by 50% in the NT2-SOA model, several factors are favorable for the SOA production. Compared to the NT-SOA model, the decrease of the enthalpy in the NT2-SOA model withholds more POG in the gas phase for oxidation. The C^* -decrease of the products by two orders of magnitude per oxidation step also increases the partitioning efficiency to the particle phase. The 40% mass increase per oxidation step further enhances the SOA production in the NT2-SOA model. The NT2-SOA model produces 66% of the observed SOA mass at T0, but the NT2-SOA model still underestimates during daytime. At T1, the NT2-SOA model improves the SOA simulations, but the underestimation is still significant in the morning from 27–29 March (Fig. 8d). In the afternoon, the NT2-SOA model remarkably enhances the SOA concentrations, showing the impacts of slow aging of the semi-volatile POA accompanied with more mass addition, but the simulations are still lower than the observation in 25 and 29 March. In terms of the RMSE and IOA at T1, the improvement of the SOA simulations in the NT2-SOA model is also significant compared to the NT-SOA model.

3.2.4 Uncertainties from OH simulations

The aging of primary organic components in the NT-SOA and NT2-SOA models is an efficient OH consumption process due to the fast reaction rate of these compounds with OH. Therefore, the aging process in the NT-SOA and NT2-SOA models inevitably decreases the OH concentration, which in turn inhibits the aging process. In order to evaluate the impacts of the aging process on the OH concentrations and further the SOA formation, we have further modified the NT-SOA and NT2-SOA models, assuming that the aging process does not have feedback on OH in the gas-phase chemistry. Hereafter, we refer to the NT-SOA and NT2-SOA models without OH feedback as the NTE-SOA and NT2E-SOA models, respectively.

Figure 9 shows the diurnal cycle of OH concentrations in the NT-SOA and NTE-SOA model at T0 and T1. Compared with the measurements at T0, the OH concentrations are substantially underestimated during morning and noontime in the NT-SOA. When the aging process does not feedback on OH in the gas-phase chemistry in the NTE-SOA model, the simulated OH concentrations are enhanced considerably, more consistent with the measurement than that in the NT-SOA model. At T1, the model frequently overestimates the observed OH concentrations in the afternoon whether the OH feedback during the aging process were included or not. The overestimation of the OH concentrations at T1 might be explained by the unsuccessful simulations of cumulus clouds that are not resolved reasonably, or the dust aerosols which frequently influence the T1 site and are not considered in the present WRF-CHEM model.

The SOA simulations are improved in the NTE-SOA and NT2E-SOA models at T0 compared with the results in the NT-SOA and NT2-SOA models, and SOA production is enhanced by around 18% and 10% during daytime, respectively (Fig. 10). The NT2E-SOA model performs better than the NTE-SOA model, and the IOA in the NT2E-SOA model is 0.86, greater than 0.78 in the NTE-SOA model. The NT2E-SOA model yields 70% of the observed SOA at T0, greater than 56% obtained by the NTE-SOA model. However, even though the aging process does not have feedback on OH in the

Simulations of organic aerosol concentrations in Mexico City

G. Li et al.

Title Page

Abstract

Introduction

Conclusions

References

Tables

Figures

⏪

⏩

◀

▶

Back

Close

Full Screen / Esc

Printer-friendly Version

Interactive Discussion



gas-phase chemistry in the NTE-SOA and NT2E-SOA models, the SOA concentrations are frequently underestimated between 08:00 and 16:00 LT. At T1, in the afternoon, the NT2E-SOA model generally reproduces the SOA concentrations on 25, 27 and 28 March, indicating that the OH enhancement accelerates the aging process efficiently.

3.2.5 Discussion

Figure 11 shows the diurnal cycles of observed and simulated POA and SOA concentrations at T0 and T1 averaged over the simulation period. At T1, the T2-SOA model significantly underestimates the observed POA concentrations but overestimates in the rest of the day. The non-traditional SOA models predict less POA mass compared to the T2-SOA model during rush hours but successfully produce the observations in the remaining time. In addition, the T2-SOA model fails to yield the high level of the observed SOA mass during daytime. The non-traditional SOA models improve the SOA simulations in the afternoon, but still underestimate the observed SOA, which is plausibly caused by missing background SOA transport. At T0, all the SOA models show good performance in simulating the POA diurnal cycles, but the modeled POA concentrations in the non-traditional SOA models are more consistent with the observations than those from the T2-SOA model during rush hours and daytime. The non-traditional SOA models still underestimate the observed SOA concentrations between 08:00 and 16:00 LT. Furthermore, among all the SOA models, the NT2E-SOA model yields the largest SOA mass, and the underestimation is about $3.0 \mu\text{g m}^{-3}$ or 21% on average between 08:00 and 16:00 LT, within the uncertainty of the AMS measurements and PMF analysis. Several sensitivity analyses have also been conducted to attempt to close the SOA gap between measurements and the WRF-CHEM model.

Impacts of dicarbonyl compounds and aromatic emissions

Figure 12 shows the SOA comparison similar to Fig. 11, except the contribution of glyoxal and methylglyoxal to the SOA formation is included in the non-traditional models.

Simulations of organic aerosol concentrations in Mexico City

G. Li et al.

Title Page

Abstract

Introduction

Conclusions

References

Tables

Figures

⏪

⏩

◀

▶

Back

Close

Full Screen / Esc

Printer-friendly Version

Interactive Discussion



Contributions of anthropogenic SOA aging

The chemical aging of the organic condensable gases produced from the oxidation of anthropogenic VOCs (hereafter referred to as OCG-AVOC) might also play an important role in the SOA formation, according to recent laboratory studies and model results (Lane et al., 2008a; Stanier et al., 2008; Donahue et al., 2006; Tsimpidi et al., 2010). In order to evaluate the SOA contribution of the aging process of the OCG-AVOC, a sensitivity study is performed based on the NT2E-SOA model, in which the OCG-AVOC is assumed to follow the same chemical aging process as POG and IVOC in Robison et al. (2007), but the rate constant with OH is reduced to $1 \times 10^{-11} \text{ cm}^3 \text{ molec}^{-1} \text{ s}^{-1}$ as given by Murphy and Pandis (2009). Inclusion of the continued aging of OCG-AVOC efficiently augments the SOA production, and the SOA mass from the anthropogenic VOCs is enhanced by 43% or $0.73 \mu\text{g m}^{-3}$ at T0 and 140% or $0.34 \mu\text{g m}^{-3}$ at T1 on average compared to the results without the aging of OCG-AVOC in the NT2E-SOA model. The aging of OCG-AVOC improves the SOA simulations compared with the measurements (Fig. 14). At T0, the underestimation between 08:00 and 16:00 LT is reduced to $1.9 \mu\text{g m}^{-3}$ or 13% on average. At T1, the simulated SOA is in good agreement with the observations in the afternoon (Fig. 14b). However, there are still uncertainties in the chemical aging of the SOA from anthropogenic VOCs (George and Abbatt, 2010).

Impacts of background transport SOA

The transport of background SOA mass can also play an important role in the evaluation of the SOA simulations (Tsimpidi et al., 2010), therefore a sensitivity study with a high SOA boundary condition of $3.5 \mu\text{g m}^{-3}$ is performed in the NT2E-SOA model. The high boundary condition improve the SOA simulation between 08:00 and 16:00 LT at T0, but causes overestimation during nighttime (Fig. 15a). At T1, the high boundary condition increase the SOA concentrations before 12:00 LT to match the measurements, but results in marked overestimation in the afternoon (Fig. 15b). In order to further verify the importance of the transport of background SOA, we also compare the observed and simulated diurnal variation of the OA mass at T2, as shown in Fig. 16.

Simulations of organic aerosol concentrations in Mexico City

G. Li et al.

Title Page

Abstract

Introduction

Conclusions

References

Tables

Figures

⏪

⏩

◀

▶

Back

Close

Full Screen / Esc

Printer-friendly Version

Interactive Discussion



nighttime O₃ and CO deviate significantly from the observation due to the difficulties in modeling the meteorological fields during nighttime and the complexity of the nighttime chemistry. The NMB and RMSE of O₃ are 20% and 11 ppb, respectively, and the IOA reaches 95%. For CO, the NMB and RMSE are 10% and 0.5 ppm, respectively, and the IOA is 84%.

The traditional SOA model performs reasonably well in simulating the POA concentrations in the urban area with the IOA of 0.81, but fails to reproduce the observed POA mass in the suburban area during rush hours. In addition, the traditional SOA model produces only around 14% of the observed SOA mass from the oxidation of anthropogenic aromatics, which is comparable to the other studies in Mexico City (Dzepina et al., 2009; Hozdic et al., 2009).

The non-traditional SOA model significantly improves the SOA simulation compared to the traditional SOA model, with more than 100% SOA enhancement, but still underestimates the observed SOA concentrations during daytime in the urban area whether using the mechanism of Robinson et al. (2009) or Grieshop et al. (2009). In the suburban area, the non-traditional SOA model still fails to reproduce the high level of observed SOA concentrations. The underestimations of SOA concentrations are principally caused by the OH treatment, emissions, aging of the SOA from anthropogenic precursors, and boundary conditions. Additionally, the non-traditional model also considerably improves POA simulations during daytime in the urban area and during the time period except rush hours in the suburban area compared to the traditional one.

In the non-traditional SOA model, the aging process of primary organic components considerably decreases the simulated OH levels, which in turn impacts the SOA formation. When the aging process does not have feedback on OH in the gas-phase chemistry in the non-traditional model, the SOA production in the non-traditional model is enhanced by more than 10% in the urban area during daytime, and the underestimation from the mechanism of Grieshop et al. (2009) is about 3.0 μg m⁻³ or 21% on average between 08:00 and 16:00 LT, within the uncertainty from the AMS measurements and PMF analysis. Glyoxal and methylglyoxal also play a role in the SOA

Simulations of organic aerosol concentrations in Mexico City

G. Li et al.

[Title Page](#)[Abstract](#)[Introduction](#)[Conclusions](#)[References](#)[Tables](#)[Figures](#)[⏪](#)[⏩](#)[◀](#)[▶](#)[Back](#)[Close](#)[Full Screen / Esc](#)[Printer-friendly Version](#)[Interactive Discussion](#)

formation and can contribute about 9.6% of the observed SOA mass in the urban area when the simulated glyoxal is in agreement with the measurements. The contribution of glyoxal and methylglyoxal help to reduce the underestimation between 08:00 and 16:00 LT in the non-traditional model without the OH feedback, and the gap is reduced to 0.87 $\mu\text{g m}^{-3}$ or 6.0% on average between 08:00 and 16:00 LT. It is noteworthy that there are large uncertainties of the SOA formation from glyoxal due to the uncertainty of the irreversible uptake coefficient of glyoxal and methylglyoxal on aerosol surfaces. The aging of the OCG-AVOC and the transport of background SOA also play an important role in the SOA evaluation.

Considering the uncertainties from measurements, emissions, meteorological conditions, aging of the SOA from anthropogenic precursors, and contributions from background transport, the non-traditional SOA model is able to close the gap in SOA mass between measurements and models.

Acknowledgements. We are indebted to the large number of people involved in the MILAGRO field campaign as well as those involved in long-term air quality monitoring and the emissions inventory in the Mexico City metropolitan area, which made this study possible, in particular, we would like to thank Jose Jimenez for making the PMF data available that we use in model comparisons. This work was supported by the US National Science Foundation's Atmospheric Chemistry Program (ATM-0528227 and ATM-0810931) and the Molina Center for Energy and the Environment. Guohui Li is a Molina Fellow at MIT. Acknowledgment is also made to the National Center for Atmospheric Research, which is sponsored by the National Science Foundation, for the computing time used in this research. The FORTH effort was supported by the European Union and the 7th Framework Programme under the project MEGAPOLI (Grant agreement no. 212520).

References

Aiken, A. C., Salcedo, D., Cubison, M. J., Huffman, J. A., DeCarlo, P. F., Ulbrich, I. M., Docherty, K. S., Sueper, D., Kimmel, J. R., Worsnop, D. R., Trimborn, A., Northway, M., Stone, E. A., Schauer, J. J., Volkamer, R. M., Fortner, E., de Foy, B., Wang, J., Laskin, A., Shutthanandan,

Simulations of organic aerosol concentrations in Mexico City

G. Li et al.

Title Page

Abstract

Introduction

Conclusions

References

Tables

Figures



Back

Close

Full Screen / Esc

Printer-friendly Version

Interactive Discussion



**Simulations of
organic aerosol
concentrations in
Mexico City**

G. Li et al.

Title Page

Abstract

Introduction

Conclusions

References

Tables

Figures

⏪

⏩

◀

▶

Back

Close

Full Screen / Esc

Printer-friendly Version

Interactive Discussion



C. D., Ziemann, P. J., and Jimenez, J. L.: Evaluation of recently-proposed secondary organic aerosol models for a case study in Mexico City, *Atmos. Chem. Phys.*, 9, 5681–5709, doi:10.5194/acp-9-5681-2009, 2009.

de Foy, B., Fast, J. D., Paech, S. J., Phillips, D., Walters, J. T., Coulter, R. L., Martin, T. J., Pekour, M. S., Shaw, W. J., Kastendeuch, P. P., Marley, N. A., Retama, A., and Molina, L. T.: Basin-scale wind transport during the MILAGRO field campaign and comparison to climatology using cluster analysis, *Atmos. Chem. Phys.*, 8, 1209–1224, doi:10.5194/acp-8-1209-2008, 2008.

de Haan, D., Corrigan, A., Smith, K., Stroik, D., Turley, J., Lee, F., Tolbert, M., Jimenez, J., and Cordova, K.: Organic aerosol-forming reactions of glyoxal with amino acids, *Environ. Sci. Technol.*, 43, 2818–2824, 2009.

de Gouw, J. A., Welsh-Bon, D., Warneke, C., Kuster, W. C., Alexander, L., Baker, A. K., Beyersdorf, A. J., Blake, D. R., Canagaratna, M., Celada, A. T., Huey, L. G., Junkermann, W., Onasch, T. B., Salcido, A., Sjostedt, S. J., Sullivan, A. P., Tanner, D. J., Vargas, O., Weber, R. J., Worsnop, D. R., Yu, X. Y., and Zaveri, R.: Emission and chemistry of organic carbon in the gas and aerosol phase at a sub-urban site near Mexico City in March 2006 during the MILAGRO study, *Atmos. Chem. Phys.*, 9, 3425–3442, doi:10.5194/acp-9-3425-2009, 2009.

DeCarlo, P. F., Dunlea, E. J., Kimmel, J. R., Aiken, A. C., Sueper, D., Crounse, J., Wennberg, P. O., Emmons, L., Shinozuka, Y., Clarke, A., Zhou, J., Tomlinson, J., Collins, D. R., Knapp, D., Weinheimer, A. J., Montzka, D. D., Campos, T., and Jimenez, J. L.: Fast airborne aerosol size and chemistry measurements above Mexico City and Central Mexico during the MILAGRO campaign, *Atmos. Chem. Phys.*, 8, 4027–4048, doi:10.5194/acp-8-4027-2008, 2008.

Donahue, N. M., Robinson, A. L., Stanier, C. O., and Pandis, S. N.: Coupled partitioning, dilution, and chemical aging of semivolatile organics, *Environ. Sci. Technol.*, 40, 2635–2643, 2006.

Fast, J., Aiken, A. C., Allan, J., Alexander, L., Campos, T., Canagaratna, M. R., Chapman, E., DeCarlo, P. F., de Foy, B., Gaffney, J., de Gouw, J., Doran, J. C., Emmons, L., Hodzic, A., Herndon, S. C., Huey, G., Jayne, J. T., Jimenez, J. L., Kleinman, L., Kuster, W., Marley, N., Russell, L., Ochoa, C., Onasch, T. B., Pekour, M., Song, C., Ulbrich, I. M., Warneke, C., Welsh-Bon, D., Wiedinmyer, C., Worsnop, D. R., Yu, X.-Y., and Zaveri, R.: Evaluating simulated primary anthropogenic and biomass burning organic aerosols during MILAGRO: implications for assessing treatments of secondary organic aerosols, *Atmos. Chem. Phys.*, 9, 6191–6215, doi:10.5194/acp-9-6191-2009, 2009.

**Simulations of
organic aerosol
concentrations in
Mexico City**

G. Li et al.

Title Page

Abstract

Introduction

Conclusions

References

Tables

Figures

◀

▶

◀

▶

Back

Close

Full Screen / Esc

Printer-friendly Version

Interactive Discussion



- Fu, T.-M., Jacob, D. J., and Heald, C. L.: Aqueous-phase reactive uptake of dicarbonyls as a source of organic aerosol over eastern North America, *Atmos. Environ.*, 43, 1814–1822, 2009.
- George, I. J. and Abbatt, J. P. D.: Chemical evolution of secondary organic aerosol from OH-initiated heterogeneous oxidation, *Atmos. Chem. Phys.*, 10, 5551–5563, doi:10.5194/acp-10-5551-2010, 2010.
- Grieshop, A. P., Logue, J. M., Donahue, N. M., and Robinson, A. L.: Laboratory investigation of photochemical oxidation of organic aerosol from wood fires 1: measurement and simulation of organic aerosol evolution, *Atmos. Chem. Phys.*, 9, 1263–1277, doi:10.5194/acp-9-1263-2009, 2009.
- Hallquist, M., Wenger, J. C., Baltensperger, U., Rudich, Y., Simpson, D., Claeys, M., Dommen, J., Donahue, N. M., George, C., Goldstein, A. H., Hamilton, J. F., Herrmann, H., Hoffmann, T., Iinuma, Y., Jang, M., Jenkin, M. E., Jimenez, J. L., Kiendler-Scharr, A., Maenhaut, W., McFiggans, G., Mentel, Th. F., Monod, A., Prévôt, A. S. H., Seinfeld, J. H., Surratt, J. D., Szmigielski, R., and Wildt, J.: The formation, properties and impact of secondary organic aerosol: current and emerging issues, *Atmos. Chem. Phys.*, 9, 5155–5236, doi:10.5194/acp-9-5155-2009, 2009.
- Harrison, R. M. and Yin, J.: Particulate matter in the atmosphere: which particle properties are important for its effects on health?, *Sci. Total Environ.*, 249, 85–101, 2000.
- Hildebrandt, L., Donahue, N. M., and Pandis, S. N.: High formation of secondary organic aerosol from the photo-oxidation of toluene, *Atmos. Chem. Phys.*, 9, 2973–2986, doi:10.5194/acp-9-2973-2009, 2009.
- Hodzic, A., Jimenez, J. L., Madronich, S., Aiken, A. C., Bessagnet, B., Curci, G., Fast, J., Lamarque, J.-F., Onasch, T. B., Roux, G., Schauer, J. J., Stone, E. A., and Ulbrich, I. M.: Modeling organic aerosols during MILAGRO: importance of biogenic secondary organic aerosols, *Atmos. Chem. Phys.*, 9, 6949–6981, doi:10.5194/acp-9-6949-2009, 2009.
- Hodzic, A., Jimenez, J. L., Madronich, S., Canagaratna, M. R., DeCarlo, P. F., Kleinman, L., and Fast, J.: Modeling organic aerosols in a megacity: potential contribution of semi-volatile and intermediate volatility primary organic compounds to secondary organic aerosol formation, *Atmos. Chem. Phys.*, 10, 5491–5514, doi:10.5194/acp-10-5491-2010, 2010.
- Horowitz, L. W., Waters, S., Mauzerall, D. L., Emmons, L. K., Rasch, P. J., Tie, X., Lamarque, J.-F., Schultz, M. G., Tyndall, G. S., Orlando, J. J., and Brasseur, G. P.: A global simulation of tropospheric ozone and related tracers: Description and evaluation of MOZART, version 2,

**Simulations of
organic aerosol
concentrations in
Mexico City**

G. Li et al.

Title Page

Abstract

Introduction

Conclusions

References

Tables

Figures

⏪

⏩

◀

▶

Back

Close

Full Screen / Esc

Printer-friendly Version

Interactive Discussion



J. Geophys. Res., 108(D24), 4784, doi:10.1029/2002JD002853, 2003.

Jimenez, J. L., Jayne, J. T., Shi, Q., Kolb, C. E., Worsnop, D. R., Yourshaw, I., Seinfeld, J. H., Flagan, R. C., Zhang, X., Smith, K. A., Morris, J. W., and Davidovits, P.: Ambient aerosol sampling using the Aerodyne Aerosol Mass Spectrometer, J. Geophys. Res., 108, 8425, doi:10.1029/2001JD001213, 2003.

Jimenez, J. L., Canagaratna, M. R., Donahue, N. M., Prevot, A. S. H., Zhang, Q., Kroll, J. H., DeCarlo, P. F., Allan, J. D., Coe, H., Ng, N. L., Aiken, A. C., Docherty, K. S., Ulbrich, I. M., Grieshop, A. P., Robinson, A. L., Duplissy, J. Smith, J. D., Wilson, K. R., Lanz, V. A., Hueglin, C., Sun, Y. L., Tian, J., Laaksonen, A., Raatikainen, T., Rautiainen, J., Vaattovaara, P., Ehn, M., Kulmala, M., Tomlinson, J. M., Collins, D. R., Cubison, M. J., Dunlea, E. J., Huffman, J. A., Onasch, T. B., Alfarra, M. R., Williams, P. I., Bower, K., Kondo, Y., Schneider, J., Drewnick, F., Borrmann, S., Weimer, S., Demerjian, K., Salcedo, D., Cottrell, L., Griffin, R., Takami, A., Miyoshi, T., Hatakeyama, S., Shimojo, A., Sun, J. Y., Zhang, Y. M., Dzepina, K., Kimmel, J. R., Sueper, D., Jayne, J. T., Herndon, S. C., Trimborn, A. M., Williams, L. R., Wood, E. C., Middlebrook, A. M., Kolb, C. E., Baltensperger, U., and Worsnop, D. R.: Evolution of organic aerosols in the atmosphere, Science, 326, 1525–1529, 2009.

Koo, B. Y., Ansari, A. S., and Pandis, S. N.: Integrated approaches to modeling the organic and inorganic atmospheric aerosol components, Atmos. Environ., 37, 4757–4768, 2003

Lane, T. E., Donahue, N. M., and Pandis, S. N.: Simulating secondary organic aerosol formation using the volatility basis-set approach in a chemical transport model, Atmos. Environ., 42, 7439–7451, 2008a.

Lane, T. E., Donahue, N. M., and Pandis, S. N.: Effect of NO_x on secondary organic aerosol concentrations, Environ. Sci. Technol., 42, 6022–6027, 2008b.

Lei, W., de Foy, B., Zavala, M., Volkamer, R., and Molina, L. T.: Characterizing ozone production in the Mexico City Metropolitan Area: a case study using a chemical transport model, Atmos. Chem. Phys., 7, 1347–1366, doi:10.5194/acp-7-1347-2007, 2007.

Lelieveld, J., Butler, T. M., Crowley, J. N., Dillon, T. J., Fischer, H., Ganzeveld, L., Harder, H., Lawrence, M. G., Martinez, M., Taraborrelli, D., and Williams, J.: Atmospheric oxidation capacity sustained by a tropical forest, Nature, 452, 737–740, 2008.

Li, G., Zhang, R., Fan, J., and Tie, X.: Impacts of black carbon aerosol on photolysis and ozone, J. Geophys. Res., 110, D23206, doi:10.1029/2005JD005898, 2005.

Li, G., Zhang, R., Fan, J., and Tie, X.: Impacts of biogenic emissions on photochemical ozone production in Houston, Texas, J. Geophys. Res., 112, D10309, doi:10.1029/2006JD007924,

2007.

Li, S., Matthews, J., and Sinha, A.: Atmospheric hydroxyl radical production from electronically excited NO₂ and H₂O, *Science*, 319, 1657–1660, 2008.

Li, G., Lei, W., Zavala, M., Volkamer, R., Dusanter, S., Stevens, P., and Molina, L. T.: Impacts of HONO sources on the photochemistry in Mexico City during the MCMA-2006/MILAGO Campaign, *Atmos. Chem. Phys.*, 10, 6551–6567, doi:10.5194/acp-10-6551-2010, 2010.

Liggio, J., Li, S.-M., and McLaren, R.: Reactive uptake of glyoxal by particulate matter, *J. Geophys. Res.*, 110, D10304, doi:10.1029/2004JD005113, 2005.

Lin Y.-L., Farley, R. D., and Orville, H. D.: Bulk parameterization of the snow field in a cloud model, *J. Appl. Meteorol.*, 22, 1065–1092, 1983.

Mlawer, E. J., Taubman, S. J., Brown, P. D., Iacono, M. J., and Clough, S. A.: Radiative transfer for inhomogeneous atmosphere: RRTM, a validated correlated-k model for the long-wave J. *Geophys. Res.*, 102(D14), 16663–16682, 1997.

Molina, L. T. and Molina, M. J.: *Air Quality in the Mexico Megacity: An Integrated Assessment*, Kluwer Academic Publishers: Dordrecht, The Netherlands, 384 pp., 2002.

Molina, L. T., Kolb, C. E., de Foy, B., Lamb, B. K., Brune, W. H., Jimenez, J. L., Ramos-Villegas, R., Sarmiento, J., Paramo-Figueroa, V. H., Cardenas, B., Gutierrez-Avedoy, V., and Molina, M. J.: Air quality in North America's most populous city – overview of the MCMA-2003 campaign, *Atmos. Chem. Phys.*, 7, 2447–2473, doi:10.5194/acp-7-2447-2007, 2007.

Molina, L. T., Madronich, S., Gaffney, J. S., Apel, E., de Foy, B., Fast, J., Ferrare, R., Herndon, S., Jimenez, J. L., Lamb, B., Osornio-Vargas, A. R., Russell, P., Schauer, J. J., Stevens, P. S., Volkamer, R., and Zavala, M.: An overview of the MILAGRO 2006 Campaign: Mexico City emissions and their transport and transformation, *Atmos. Chem. Phys.*, 10, 8697–8760, doi:10.5194/acp-10-8697-2010, 2010.

Murphy, B. N. and Pandis, S. N.: Simulating the formation of semivolatile primary and secondary aerosol in a regional chemical transport model, *Environ. Sci. Technol.*, 43, 4722–4728, 2009.

Ng, N. L., Kroll, J. H., Keywood, M. D., Bahreini, R., Varutbangkul, V., Flagan, R. C., and Seinfeld, J. H.: Contribution of first-versus second-generation products to secondary organic aerosols formed in the oxidation of biogenic hydrocarbons, *Environ. Sci. Technol.*, 40, 2283–2297, 2006.

Ng, N. L., Kroll, J. H., Chan, A. W. H., Chhabra, P. S., Flagan, R. C., and Seinfeld, J. H.: Secondary organic aerosol formation from m-xylene, toluene, and benzene, *Atmos. Chem.*

Simulations of organic aerosol concentrations in Mexico City

G. Li et al.

Title Page

Abstract

Introduction

Conclusions

References

Tables

Figures

⏪

⏩

◀

▶

Back

Close

Full Screen / Esc

Printer-friendly Version

Interactive Discussion



Simulations of organic aerosol concentrations in Mexico City

G. Li et al.

Title Page

Abstract

Introduction

Conclusions

References

Tables

Figures

◀

▶

◀

▶

Back

Close

Full Screen / Esc

Printer-friendly Version

Interactive Discussion



Phys., 7, 3909–3922, doi:10.5194/acp-7-3909-2007, 2007.

Noh, Y., Cheon, W. G., and Raasch, S.: The improvement of the K-profile model for the PBL using LES. Preprints, Int. Workshop of Next Generation NWP Models, Seoul, South Korea, Laboratory for Atmospheric Modeling Research, 65–66, 2001.

5 Odum, J. R., Hoffman, T., Bowman, F., Collins, D., Flagan, R. C., and Seinfeld, J. H.: Gas/particle partitioning and secondary organic aerosol yields, *Environ. Sci. Technol.*, 30, 2580–2585, 1996.

Pankow, J. F.: An absorption model of gas/particle partitioning involved in the formation of secondary organic aerosol, *Atmos. Environ.*, 28, 189–193, 1994.

10 Penner, J. E., Andreae, M. O., Annegarn, H., Barrie, L., Feichter, J., Hegg, D., Jayaraman, A., Leaitch, R., Murphy, D., Nganga, J., and Pitari, G.: Aerosols, their direct and indirect effects, in *Climate Change 2001: The Scientific Basis*, edited by: Houghton, J. T., Ding, Y., Griggs, D. J., Noguer, M., van der Linden, P. J., Dai, X., Maskell K., and Johnson, C. A., Cambridge Univ. Press, New York, 289–348, 2001.

15 Pope III, C. A. and Dockery, D. W.: Health effects of fine particulate air pollution: Liens that connect, *J. Air. Waste Manage*, 56, 709–742, 2006.

Robinson, A. L., Donahue, N.M., Shrivastava, M. K., Weitkamp, E. A., Sage, A. M., Grieshop, A. P., Lane, T. E., Pandis, S. N., and Pierce, J. R.: Rethinking organic aerosols: semivolatile emissions and photochemical aging, *Science*, 315, 1259–1262, 2007.

20 Sareen, N., Schwier, A. N., Shapiro, E. L., Mitroo, D., and McNeill, V. F.: Secondary organic material formed by methylglyoxal in aqueous aerosol mimics, *Atmos. Chem. Phys.*, 10, 997–1016, doi:10.5194/acp-10-997-2010, 2010.

Schell, B., Ackermann, I. J., Hass, H., Binkowski, F. S., and Ebel, A.: Modeling the formation of secondary organic aerosol within a comprehensive air quality modeling system, *J. Geophys. Res.*, 106, 28275–28293, 2001.

25 Shrivastava, M. K., Lane, T. E., Donahue, N. M., Pandis, S. N., and Robinson, A. L.: Effects of gas-particle partitioning and aging of primary emissions on urban and regional organic aerosol concentrations, *J. Geophys. Res.*, 113, D18301, doi:10.1029/2007JD009735, 2008.

30 Song, J., Lei, W., Bei, N., Zavala, M., de Foy, B., Volkamer, R., Cardenas, B., Zheng, J., Zhang, R., and Molina, L. T.: Ozone response to emission changes: a modeling study during the MCMA-2006/MILAGRO Campaign, *Atmos. Chem. Phys.*, 10, 3827–3846, doi:10.5194/acp-10-3827-2010, 2010.

Stanier, C. O., Donahue, N. M., and Pandis, S. N.: Parameterization of secondary organic

**Simulations of
organic aerosol
concentrations in
Mexico City**

G. Li et al.

Title Page

Abstract

Introduction

Conclusions

References

Tables

Figures

⏪

⏩

◀

▶

Back

Close

Full Screen / Esc

Printer-friendly Version

Interactive Discussion



aerosol mass fraction from smog chamber data, *Atmos. Environ.*, 42, 2276–2299, 2008.

Tie, X., Madronich, S., Walters, S., Zhang, R., Rasch, P., and Collins, W.: Effect of clouds on photolysis and oxidants in the troposphere, *J. Geophys. Res.*, 108(D20), 4642, doi:10.1029/2003JD003659, 2003.

5 Tsimpidi, A. P., Karydis, V. A., Zavala, M., Lei, W., Molina, L., Ulbrich, I. M., Jimenez, J. L., and Pandis, S. N.: Evaluation of the volatility basis-set approach for the simulation of organic aerosol formation in the Mexico City metropolitan area, *Atmos. Chem. Phys.*, 10, 525–546, doi:10.5194/acp-10-525-2010, 2010.

10 Volkamer, R., Jimenez, J. L., San Martini, F., Dzepina, K., Zhang, Q., Salcedo, D., Molina, L. T., Worsnop, D. R., and Molina, M. J.: Secondary organic aerosol formation from anthropogenic air pollution: rapid and higher than expected, *Geophys. Res. Lett.*, 33, L17811, doi:10.1029/2006GL026899, 2006.

Volkamer, R., San Martini, F., Molina, L. T., Salcedo, D., Jimenez, J. L., and Molina, M. J.: A Missing Sink for Gas-Phase Glyoxal in Mexico City: Formation of Secondary Organic Aerosol, *Geophys. Res. Lett.*, 34, L19807, doi:10.1029/2007GL030752, 2007.

15 Wesely, M. L.: Parameterization of surface resistance to gaseous dry deposition in regional-scale numerical models, *Atmos. Environ.*, 23, 1293–1304, 1989.

Zhang, Y., Liu, P., Queen, A., Misenis, C., Pun, B., Seigneur, C., Wu, and S. Y.: A comprehensive performance evaluation of MM5-CMAQ for the summer 1999 Southern Oxidants Study episode. Part II: gas and aerosol predictions, *Atmos. Environ.*, 40(26), 4839–4855, 2006.

20 Zhang, R., Li, G., Fan, J., Wu, D. L., and Molina, M. J.: Intensification of Pacific storm track linked to Asian pollution, *P. Natl. Acad. Sci. USA*, 104, 5295–5299, doi:10.1073/pnas.0700618104, 2007a.

Zhang, Q., Jimenez, J. L., Canagaratna, M. R., Allan, J. D., Coe, H., Ulbrich, I., Alfarra, M. R., Takami, A., Middlebrook, A. M., Sun, Y. L., Dzepina, K., Dunlea, E., Docherty, K., DeCarlo, P. F., Salcedo, D., Onasch, T., Jayne, J. T., Miyoshi, T., Shimonono, A., Hatakeyama, S., Takegawa, N., Kondo, Y., Schneider, J., Drewnick, F., Borrmann, S., Weimer, S., Demerjian, K., Williams, P., Bower, K., Bahreini, R., Cottrell, L., Griffin, R. J., Rautiainen, J., Sun, J. Y., Zhang, Y. M., and Worsnop, D. R.: Ubiquity and dominance of oxygenated species in organic aerosols in anthropogenically-influenced Northern Hemisphere midlatitudes, *Geophys. Res. Lett.*, 34, L13801, doi:10.1029/2007GL029979, 2007b.

30 Zhang, Y., Dubey, M. K., Olsen, S. C., Zheng, J., and Zhang, R.: Comparisons of WRF/Chem simulations in Mexico City with ground-based RAMA measurements during the 2006-

- MILAGRO, Atmos. Chem. Phys., 9, 3777–3798, doi:10.5194/acp-9-3777-2009, 2009.
- Zhao, J., Levitt, N. P., Zhang, R. Y., and Chen, J. M.: Heterogeneous reactions of methylglyoxal in acidic media: implications for secondary organic aerosol formation, Environ. Sci. Technol., 40, 7682–7687, 2006.
- 5 Zheng, J., Zhang, R., Fortner, E. C., Volkamer, R. M., Molina, L., Aiken, A. C., Jimenez, J. L., Gaeggeler, K., Dommen, J., Dusanter, S., Stevens, P. S., and Tie, X.: Measurements of HNO₃ and N₂O₅ using ion drift-chemical ionization mass spectrometry during the MILAGRO/MCMA-2006 campaign, Atmos. Chem. Phys., 8, 6823–6838, doi:10.5194/acp-8-6823-2008, 2008.

Simulations of organic aerosol concentrations in Mexico City

G. Li et al.

Title Page

Abstract

Introduction

Conclusions

References

Tables

Figures

⏪

⏩

◀

▶

Back

Close

Full Screen / Esc

Printer-friendly Version

Interactive Discussion



Simulations of organic aerosol concentrations in Mexico City

G. Li et al.

[Title Page](#)[Abstract](#)[Introduction](#)[Conclusions](#)[References](#)[Tables](#)[Figures](#)[⏪](#)[⏩](#)[◀](#)[▶](#)[Back](#)[Close](#)[Full Screen / Esc](#)[Printer-friendly Version](#)[Interactive Discussion](#)

Table 2. Statistical comparison of measured SOA concentrations and simulations from sensitivity studies based on the NT2E-SOA model at T0 and T1 during the period from 24 to 29 March 2006.

Case	Urban Site (T0)				Suburban Site (T1)			
	BA ¹	AD ²	VA ³	HB ⁴	BA ¹	AD ²	VA ³	HB ⁴
SOA								
NMB (%)	−12	1.3	−3.0	8.9	−32	−27	−24	3.3
RMSE ($\mu\text{g m}^{-3}$)	3.7	3.4	3.6	3.8	2.2	2.1	2.1	1.6
IOA	0.86	0.90	0.88	0.88	0.67	0.68	0.69	0.77

¹ Base case (the NT2E-SOA model); ² adjustment case with the doubled glyoxal yield from ARO1 and ARO2 and 30% increase of ARO2 emissions in the NT2E SOA model. The SOA formation from glyoxal and methylglyoxal is included; ³ the SOA from the oxidation of VOCs is aging with the reaction rate of $1 \times 10^{-11} \text{ cm}^3 \text{ molec}^{-1} \text{ s}^{-1}$ with OH in the NT2E-SOA model; ⁴ High Background case with the background SOA of $3.5 \mu\text{g m}^{-3}$ in the NT2E-SOA model.

**Simulations of
organic aerosol
concentrations in
Mexico City**

G. Li et al.

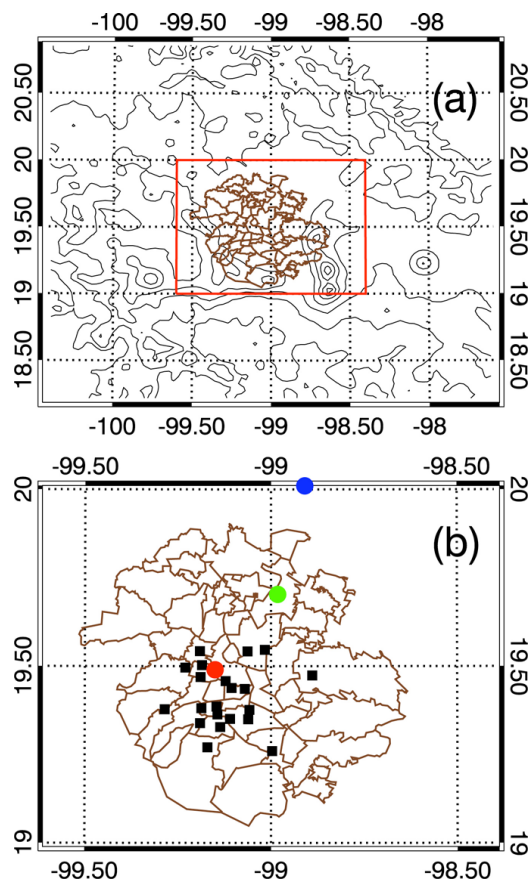


Fig. 1. WRF-CHEM simulation domain. Black squares represent the RAMA (Mexico City Ambient Air Monitoring Network) sites. The red, blue, and green circles represent the T0, T1, and T2 supersites, respectively.

[Title Page](#)[Abstract](#)[Introduction](#)[Conclusions](#)[References](#)[Tables](#)[Figures](#)[◀](#)[▶](#)[◀](#)[▶](#)[Back](#)[Close](#)[Full Screen / Esc](#)[Printer-friendly Version](#)[Interactive Discussion](#)

Simulations of organic aerosol concentrations in Mexico City

G. Li et al.

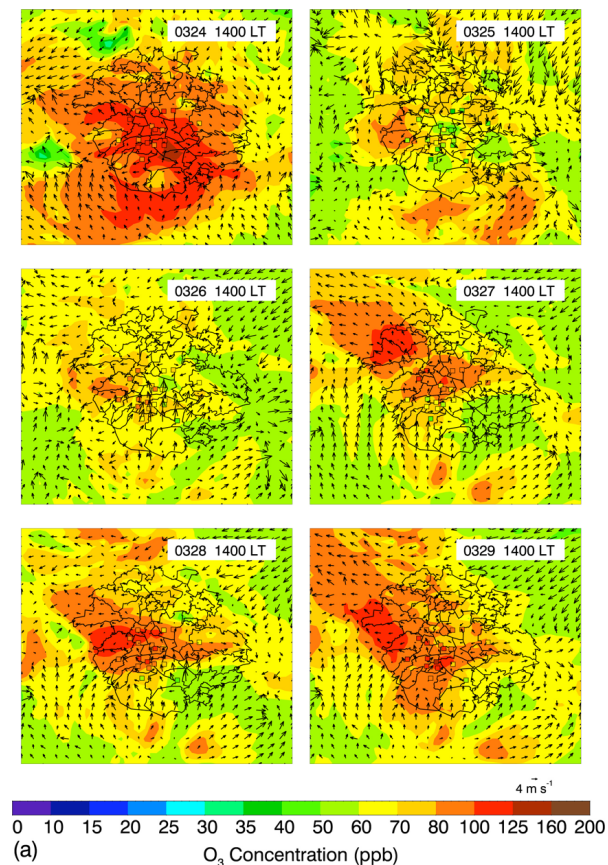


Fig. 2. Pattern comparison of simulated vs. observed O₃ at 14:00 and 17:00 LT over Mexico City during the period from 24 to 29 March 2006. Colored squares: O₃ observations; color contour: O₃ simulations in the NT-SOA model; black arrows: simulated surface winds.

[Title Page](#)[Abstract](#)[Introduction](#)[Conclusions](#)[References](#)[Tables](#)[Figures](#)[◀](#)[▶](#)[◀](#)[▶](#)[Back](#)[Close](#)[Full Screen / Esc](#)[Printer-friendly Version](#)[Interactive Discussion](#)

Simulations of organic aerosol concentrations in Mexico City

G. Li et al.

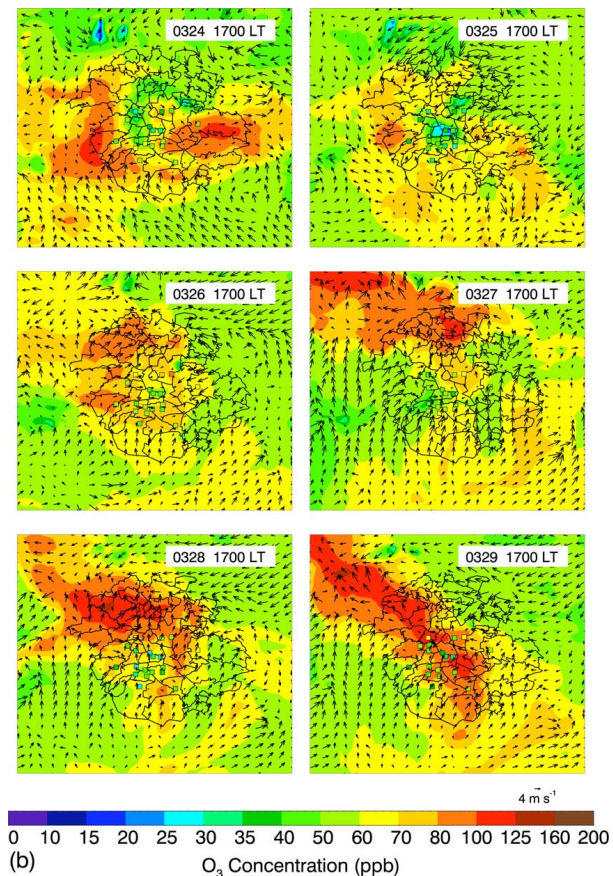


Fig. 2. Continued.

Title Page	
Abstract	Introduction
Conclusions	References
Tables	Figures
◀	▶
◀	▶
Back	Close
Full Screen / Esc	
Printer-friendly Version	
Interactive Discussion	

Simulations of
organic aerosol
concentrations in
Mexico City

G. Li et al.

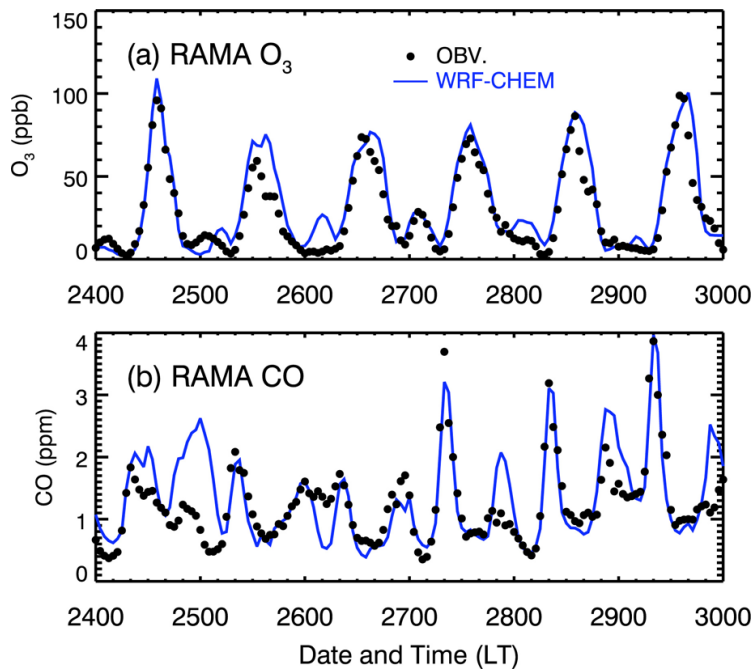


Fig. 3. Comparison of measured (black dots) and simulated (blue line) diurnal variations of near surface hourly **(a)** O_3 and **(b)** CO concentrations averaged over all monitoring sites.

[Title Page](#)[Abstract](#)[Introduction](#)[Conclusions](#)[References](#)[Tables](#)[Figures](#)[◀](#)[▶](#)[◀](#)[▶](#)[Back](#)[Close](#)[Full Screen / Esc](#)[Printer-friendly Version](#)[Interactive Discussion](#)

Simulations of
organic aerosol
concentrations in
Mexico City

G. Li et al.

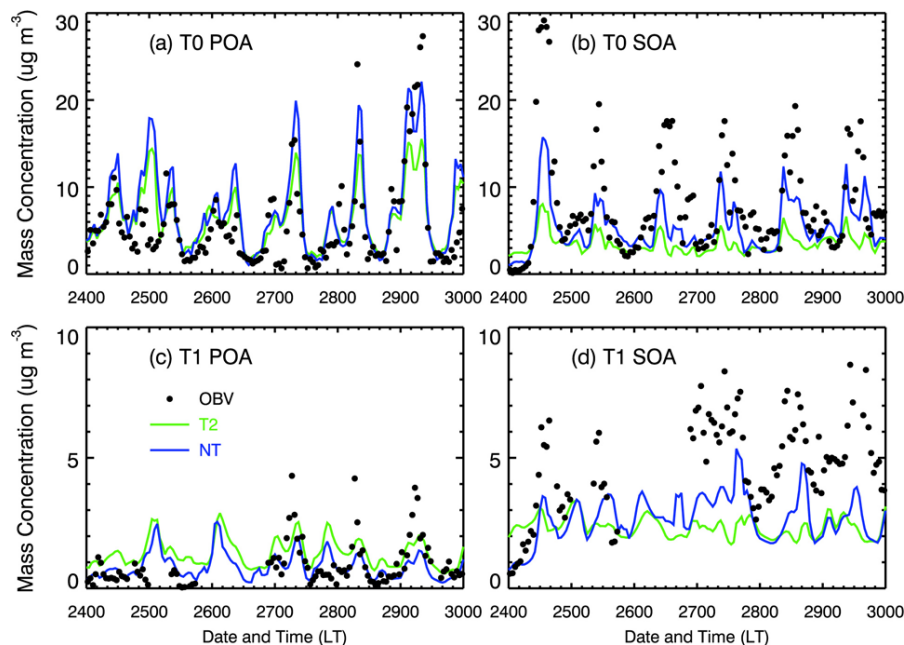


Fig. 4. Diurnal variations of measured and simulated organic aerosol concentrations at T0 and T1 during the period from 24 to 29 March 2006. **(a)** POA at T0, **(b)** SOA at T0, **(c)** POA at T1, and **(d)** SOA at T1. Black dots: measurements; green line: the T2-SOA model; Blue line: the NT-SOA model.

Title Page

Abstract

Introduction

Conclusions

References

Tables

Figures

◀

▶

◀

▶

Back

Close

Full Screen / Esc

Printer-friendly Version

Interactive Discussion

**Simulations of
organic aerosol
concentrations in
Mexico City**

G. Li et al.

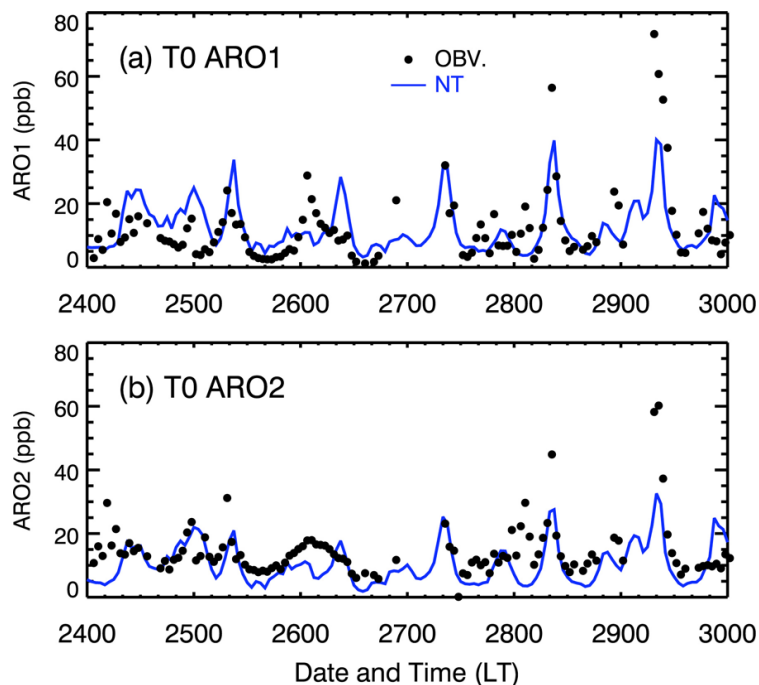
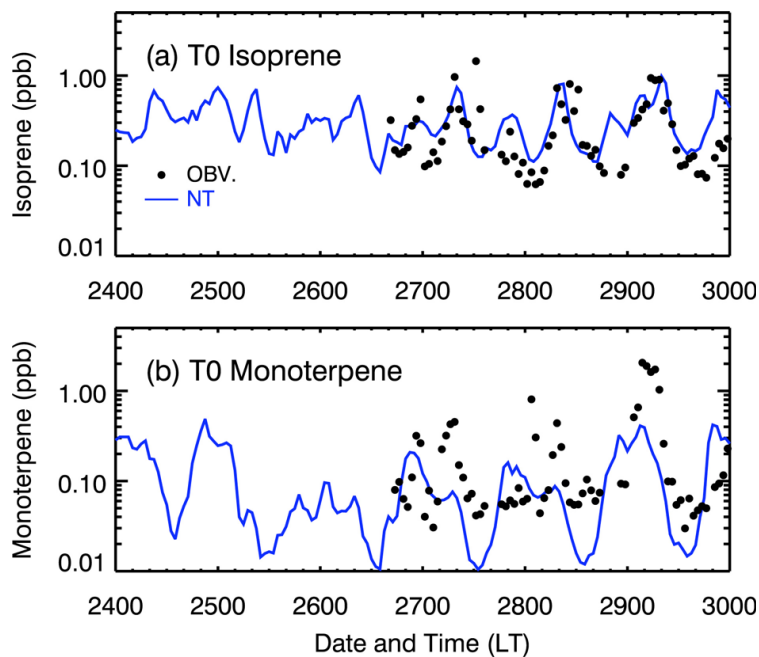


Fig. 5. Comparison of simulated (a) ARO1 and (b) ARO2 with measurements at T0 during the period from 24 to 29 March 2006. Black dots: measurements; blue line: the NT-SOA model simulations.

[Title Page](#)[Abstract](#)[Introduction](#)[Conclusions](#)[References](#)[Tables](#)[Figures](#)[◀](#)[▶](#)[◀](#)[▶](#)[Back](#)[Close](#)[Full Screen / Esc](#)[Printer-friendly Version](#)[Interactive Discussion](#)

**Simulations of
organic aerosol
concentrations in
Mexico City**

G. Li et al.

**Fig. 6.** Same as Fig. 6, except for **(a)** isoprene and **(b)** monoterpene.[Title Page](#)[Abstract](#)[Introduction](#)[Conclusions](#)[References](#)[Tables](#)[Figures](#)[◀](#)[▶](#)[◀](#)[▶](#)[Back](#)[Close](#)[Full Screen / Esc](#)[Printer-friendly Version](#)[Interactive Discussion](#)

Simulations of
organic aerosol
concentrations in
Mexico City

G. Li et al.

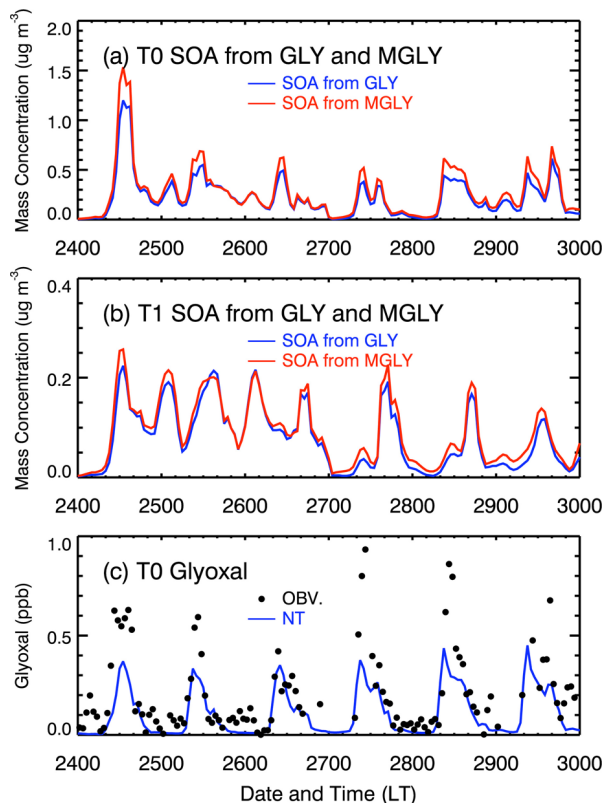


Fig. 7. Diurnal variations of **(a)** SOA concentrations from glyoxal and methylglyoxal at T0, **(b)** at T1, and **(c)** glyoxal concentrations at T0. In (a) and (b), the red and blue lines represent the SOA contributions from glyoxal and methylglyoxal, respectively. In (c), black dots are measurements and blue line denotes the simulations in the NT-SOA model.

Simulations of organic aerosol concentrations in Mexico City

G. Li et al.

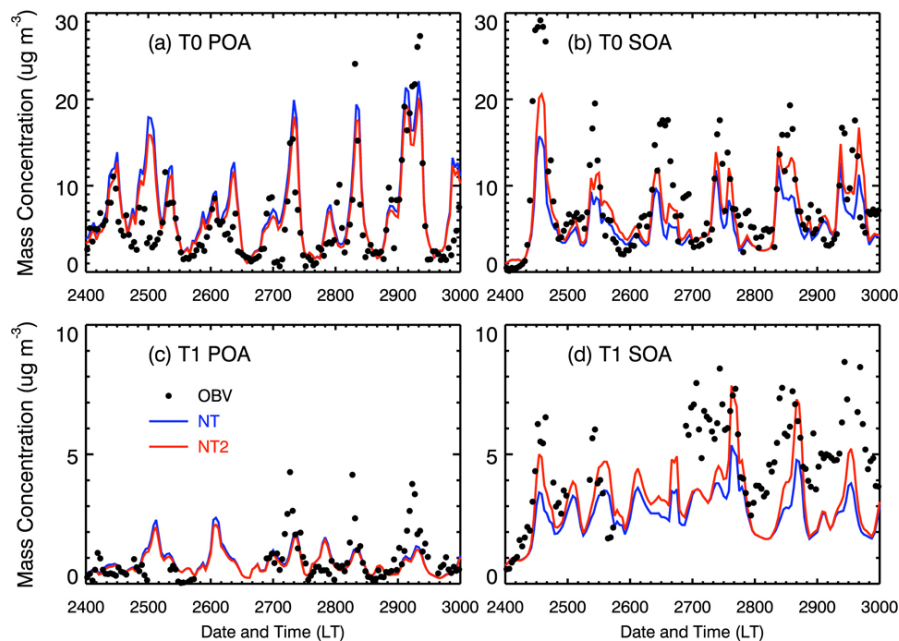


Fig. 8. Same as Fig. 4, except that the blue line represents the NT-SOA model and the red line denotes the NT2-SOA model.

[Title Page](#)[Abstract](#)[Introduction](#)[Conclusions](#)[References](#)[Tables](#)[Figures](#)[◀](#)[▶](#)[◀](#)[▶](#)[Back](#)[Close](#)[Full Screen / Esc](#)[Printer-friendly Version](#)[Interactive Discussion](#)

Simulations of
organic aerosol
concentrations in
Mexico City

G. Li et al.

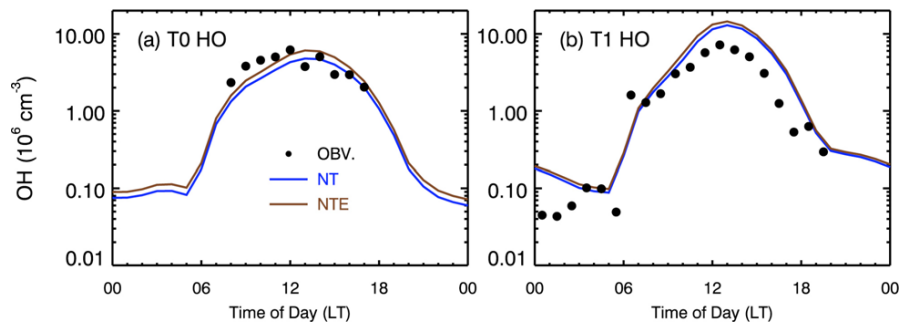


Fig. 9. OH diurnal cycles **(a)** at T0 and **(b)** at T1 averaged during the period from 24 to 29 March 2006. Black dots: measurements; blue line: the NT-SOA model; brown line: the NTE-SOA model (without OH feedback).

[Title Page](#)[Abstract](#)[Introduction](#)[Conclusions](#)[References](#)[Tables](#)[Figures](#)[◀](#)[▶](#)[◀](#)[▶](#)[Back](#)[Close](#)[Full Screen / Esc](#)[Printer-friendly Version](#)[Interactive Discussion](#)

Simulations of organic aerosol concentrations in Mexico City

G. Li et al.

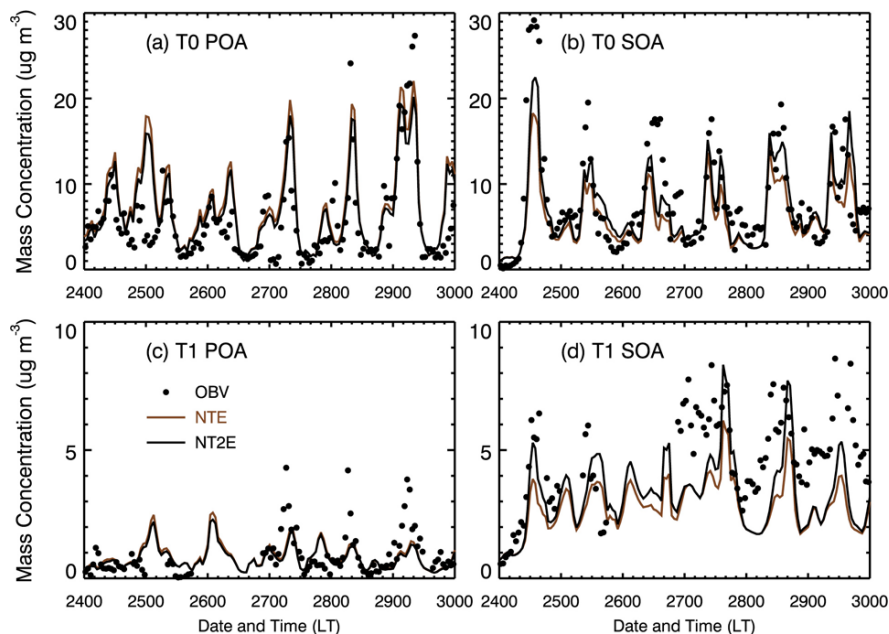


Fig. 10. Same as Fig. 4, except that the brown line represents the NTE-SOA model (without OH feedback) and the black line denotes the NT2E-SOA model (without OH feedback).

[Title Page](#)[Abstract](#)[Introduction](#)[Conclusions](#)[References](#)[Tables](#)[Figures](#)[◀](#)[▶](#)[◀](#)[▶](#)[Back](#)[Close](#)[Full Screen / Esc](#)[Printer-friendly Version](#)[Interactive Discussion](#)

Simulations of organic aerosol concentrations in Mexico City

G. Li et al.

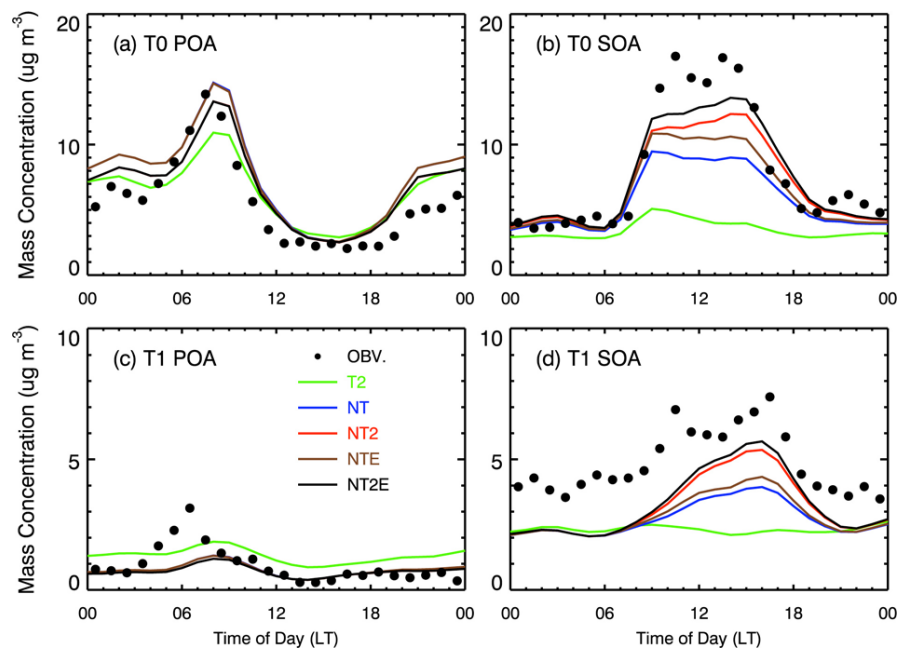


Fig. 11. Diurnal cycles of measured and simulated organic aerosol concentrations at T0 and T1 averaged during the period from 24 to 29 March 2006. **(a)** POA at T0, **(b)** SOA at T0, **(c)** POA at T1, and **(d)** SOA at T1. Black dots: measurements; green line: the T2-SOA model; blue line: the NT-SOA model; red line: the NT2-SOA model; brown line: the NTE-SOA model; black line: the NT2E-SOA model.

[Title Page](#)
[Abstract](#)
[Introduction](#)
[Conclusions](#)
[References](#)
[Tables](#)
[Figures](#)
[⏪](#)
[⏩](#)
[◀](#)
[▶](#)
[Back](#)
[Close](#)
[Full Screen / Esc](#)
[Printer-friendly Version](#)
[Interactive Discussion](#)

Simulations of organic aerosol concentrations in Mexico City

G. Li et al.

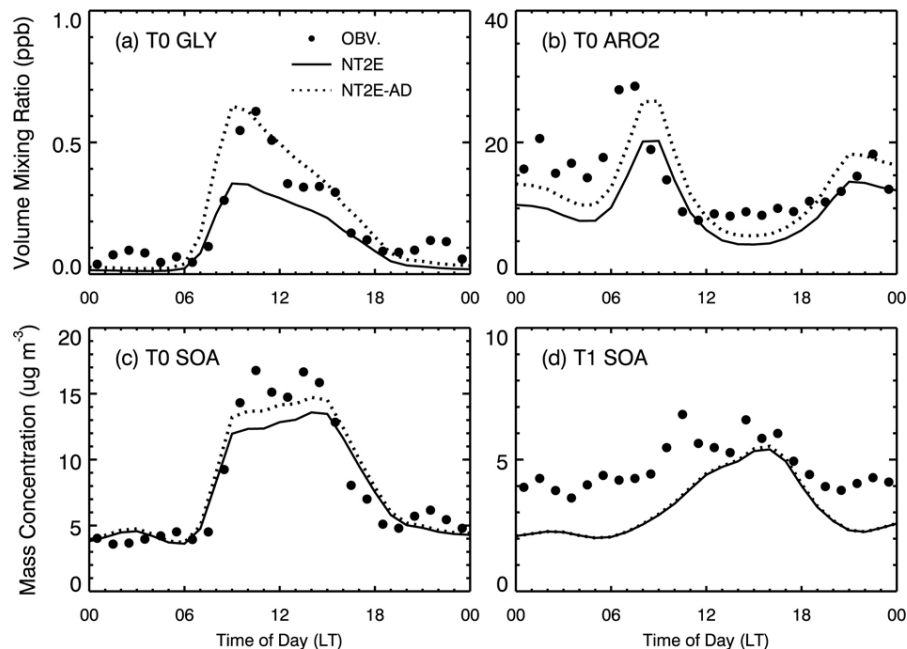


Fig. 13. Diurnal cycles of (a) ARO2 at T0, (b) glyoxal at T0, (c) SOA at T0, and (d) SOA at T1 averaged during the period from 24 to 29 March 2006. Black dots: measurements; black solid line: the NT2E-SOA model; black dotted line: NT2E-SOA model with high yield glyoxal from ARO1 and ARO2 and increased ARO2 emissions.

[Title Page](#)
[Abstract](#)
[Introduction](#)
[Conclusions](#)
[References](#)
[Tables](#)
[Figures](#)
[Back](#)
[Close](#)
[Full Screen / Esc](#)
[Printer-friendly Version](#)
[Interactive Discussion](#)

Simulations of organic aerosol concentrations in Mexico City

G. Li et al.

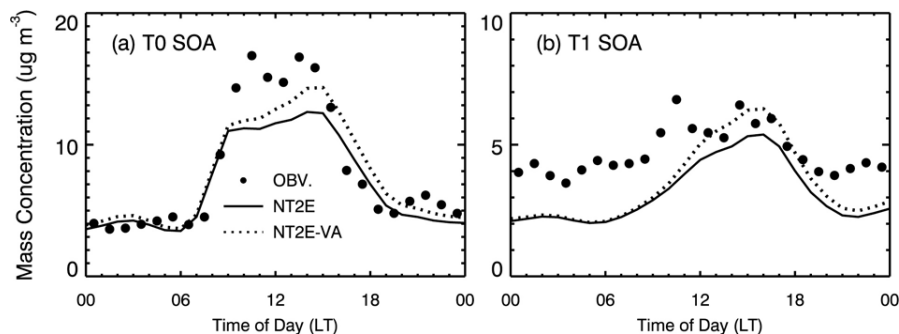


Fig. 14. Diurnal cycles of SOA (a) T0 and (b) at T1 averaged during the period from 24 to 29 March 2006. Black dots: measurements; black solid line: the NT2E-SOA model; black dotted line: NT2E-SOA model with the aging of the organic condensable gases from the oxidation of anthropogenic precursors.

[Title Page](#)[Abstract](#)[Introduction](#)[Conclusions](#)[References](#)[Tables](#)[Figures](#)[⏪](#)[⏩](#)[◀](#)[▶](#)[Back](#)[Close](#)[Full Screen / Esc](#)[Printer-friendly Version](#)[Interactive Discussion](#)

Simulations of organic aerosol concentrations in Mexico City

G. Li et al.

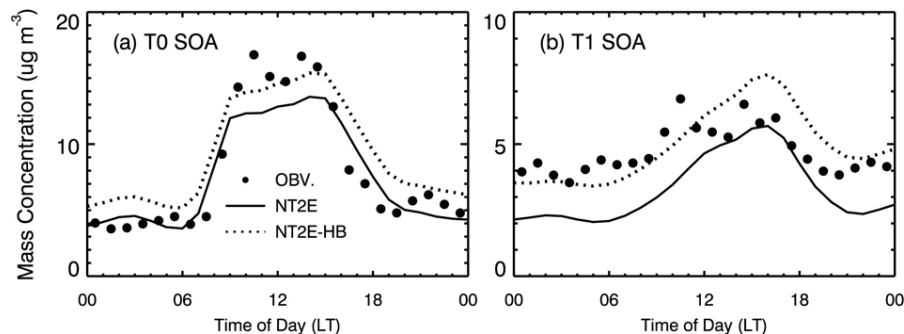


Fig. 15. Diurnal cycles of SOA (a) T0 and (b) at T1 averaged during the period from 24 to 29 March 2006. Black dots: measurements; black solid line: the NT2E-SOA model; black dotted line: NT2E-SOA model with high background SOA.

[Title Page](#)[Abstract](#)[Introduction](#)[Conclusions](#)[References](#)[Tables](#)[Figures](#)[⏪](#)[⏩](#)[◀](#)[▶](#)[Back](#)[Close](#)[Full Screen / Esc](#)[Printer-friendly Version](#)[Interactive Discussion](#)

**Simulations of
organic aerosol
concentrations in
Mexico City**

G. Li et al.

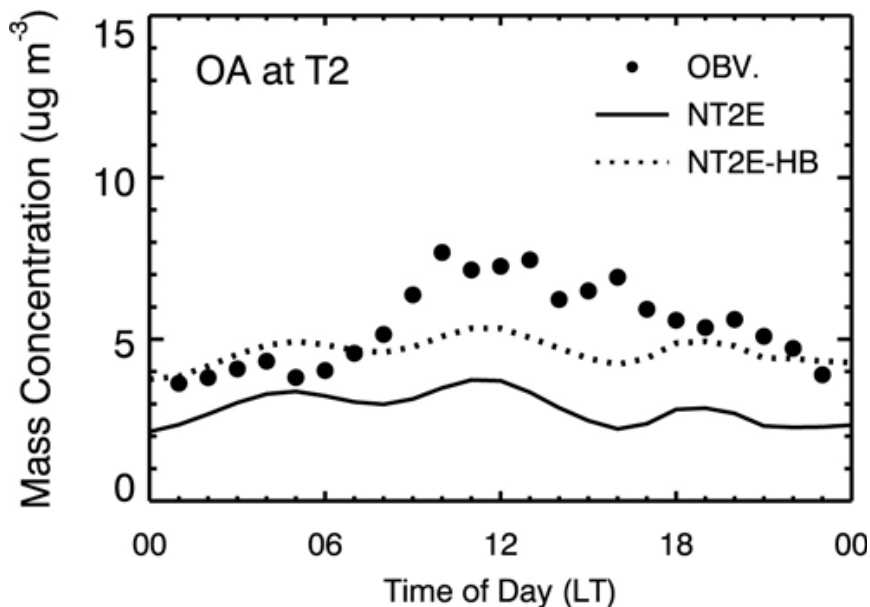


Fig. 16. Diurnal cycles of OA at T2 averaged during the period from 24 to 29 March 2006. Black dots: measurements; black solid line: the NT2E-SOA model; black dotted line: NT2E-SOA model with high background SOA.

[Title Page](#)[Abstract](#)[Introduction](#)[Conclusions](#)[References](#)[Tables](#)[Figures](#)[⏪](#)[⏩](#)[◀](#)[▶](#)[Back](#)[Close](#)[Full Screen / Esc](#)[Printer-friendly Version](#)[Interactive Discussion](#)